STUDY OF RESIDUAL STRESS AND MICROSTRUCTURE EVOLUTION IN MAGNESIUM ALLOY (WE43) DUE TO DEFORMATION PROCESS VIA (PTCAP)

MAHMOUD SARHAN SADDAM OWN

RESEARCH REPORT SUBMITTED TO THE FACULTY OF ENGINEERING UNIVERSITY OF MALAYA, IN PARTIAL FULFILMENT OF THE REQUIREMENTS FOR THE DEGREE OF MANUFACTURING ENGINEERING

2018

University of Malaya

UNIVERSITY OF MALAYA
ORIGINAL LITERARY WORK DECLARATION

Name of Candidate: MAHMOUD SARHAN SADDAM

Matric No: KQG160008

Name of Degree: Master of Manufacturing Engineering

STUDY OF RESIDUAL STRESS AND MICROSTRUCTURE EVOLUTION IN MAGNESIUME ALLOY (WE43) DUE TO DEFORMATION PROCESS VIA (PTCAP)

Field of Study: Surface Engineering

I do solemnly and sincerely declare that:

(1) I am the sole author/writer of this Work;
(2) This Work is original;
(3) Any use of any work in which copyright exists was done by way of fair dealing and for permitted purposes and any excerpt or extract from, or reference to or reproduction of any copyright work has been disclosed expressly and sufficiently and the title of the Work and its authorship have been acknowledged in this Work;
(4) I do not have any actual knowledge nor do I ought reasonably to know that the making of this work constitutes an infringement of any copyright work;
(5) I hereby assign all and every rights in the copyright to this Work to the University of Malaya ("UM"), who henceforth shall be owner of the copyright in this Work and that any reproduction or use in any form or by any means whatsoever is prohibited without the written consent of UM having been first had and obtained;
(6) I am fully aware that if in the course of making this Work I have infringed any copyright whether intentionally or otherwise, I may be subject to legal action or any other action as may be determined by UM.

Candidate's Signature Date:

Subscribed and solemnly declared before,

Witness's Signature Date:

Name:

Designation

University of Malaya

ABSTRACT

In advanced industries, the demand of light and efficient parts in terms of structural integrity under particular mechanical purpose and aggressive environmental conditions has increased. Thus, requirement for a creative process that is aimed to upgrade metal material properties without adding additional weight or additives to the metal was a must. Several processes are categorized under the Severe Plastic Deformation (SPD) such as equal channel angular extrusion (ECAE), another method called equal channel angular pressing (ECAP), as well as high pressure torsion (HPT), and Parallel Tubular channel angular pressing (PTCAP). PTCAP is a recently developed and powerful plastic deformation method that is used to enhance the mechanical properties of the processed tubes. Residual stresses are generated inside the processed tubes during the deformation processes and could significantly influence or affect the mechanical performance of the final part. Thus, the effects of deformation process on residual stress, strain and to the crystallite size of Magnesium Alloy tubes was examined by means of X-Ray Diffraction (XRD). The results have shown that: residual stress was clearly changed from tensile stress before the deformation to compressive stress after the deformation process which means more crack resistance and better performance; the crystallite size shows reduction from 20.39 nm before the deformation process to 14.33 nm after 3rd pass. In addition, the approximation and Williamson Hall equations were compared in terms of strain percentage and crystallite size to evaluate the effectiveness of the Approximation method on crystallite size and strain calculation. Approximation method was found to give higher values than Williamson Hall.

University of Malaya

ABSTRAK

Dalam industri-industri maju, permintaan untuk bahagian yang ringan dan cekap dari segi integriti struktur di bawah keadaan mekanikal tertentu dan persekitaran yang agresif telah meningkat. Beberapa proses dikategorikan di bawah Ubah Bentuk Plastik Teruk seperti pemyemperitan bersudut saluran sama, kaedah lain yang dinamakan penekanan bersudut saluran sama (ECAP), serta kilasan tekenan tinggi (HPT), dan penekanan bersudut saluran tiub selari (PTCAP). PTCAP adalah kaedah ubah bentuk plastik yang baru dibangunkan yang dignakan untuk meningkatkan sifat-sifat mekanikal tiub yang diproses. Tegasan sisa dijanakan dalam bahan semasa proses ubah bentuk dan boleh mempengaruhi secara ketara sifat-sifat mekanikal produk terakhir. Oleh itu, kesan ubah bentuk pada tegasan sisa, ketegangan dan pengecilan saiz bijian aloi magnesium telah diperiksa dengan menggunakan Difraksi Sinar-X (XRD). Selain itu, teknik analisis unsur terhingga telah digunakan untuk menyokong penemuan hasil tekanan. Keputusan telah menunjukkan bahawa tegasan sisa telah berubah dengan jelas dari tegasan mampatan sebelum ubah bentuk kepada tekanan tegangan selepas proses ubah bentuk, dan saiz bijian menunjukkan pengurangan dari 20.39 nm sebelum itu kepada 14.33 nm selepas kelulusan ke-3. Di samping itu, penghampiran dan persamaan Williamson Hall dibandingkan dari segi hasil. Kaedah penghampiran didapati memberikan nilai yang lebih tinggi daripada kaedah Williamson Hall.

University of Malaya

ACKNOWLEDGEMENTS

I would first like to thank my project research advisor Associate Prof. Dr. Bushroa Binti Abdul Razak of the Faculty of engineering University of Malaya. The door to Prof. Bushroa's office was always open whenever I ran into a trouble spot or had a question about my research or writing. She consistently allowed this project to be my own work but steered me in the right direction whenever she thought I needed it.

I would also like to thank Mr. Mohsen Mesbah who was involved in the preparation of the samples and act as a mentor for this research project. Without his generous participation and input, the experimental test could not have been successfully conducted.

I would also like to acknowledge Ir. Dr. Tan Chin Joo, and Dr. Suriani Ibrahim of the Faculty of engineering at University of Malay as the examiners of this research, and I am gratefully indebted to their very valuable comments on this research.

Finally, I must express my deep thanks to all University of Malaya lecturers and staff that I have met throughout my years of study and through the process of researching and writing this project. This accomplishment would not have been possible without them. Thank you.

University of Malaya

DEDICATIONS

I dedicate this project to God Almighty my creator, my strong pillar, my source of inspiration, wisdom, knowledge and understanding. He has been the source of my strength throughout this program. I also dedicate this work and express my very profound gratitude to my parents; who have supported and encouraged me all the way and whose encouragement has made sure that I give it all it takes to finish what I have started. To my wife Nada and my son Majd who have been affected in every way possible by this quest. Thank you. My love for you all can never be quantified. God bless you.

University of Malaya

TABLE OF CONTENTS

University of Malaya

University of Malaya

LIST OF FIGURES

University of Malaya

University of Malaya

LIST OF TABLES

University of Malaya

LIST OF SYMBOLS AND ABBREVIATIONS

Symbol	Definition
ECAE	Equal channel angular extrusion
ECAP	Equal channel angular pressing
HCP	hexagonal closed packed
HPT	High pressure torsion
PTCAP	parallel tubular channel angular pressing
SPD	Severe plastic deformation
TCAP	tubular channel angular pressing
XRD	X-Ray Diffraction
$\mathbf{S_0}$	Zero pass
$\mathbf{S_1}$	First pass
$\mathbf{S_2}$	Second pass
$\mathbf{S_3}$	Third pass
a, b, c, α, β, γ	vectors; a, b, c, which define the crystallographic axes of a unit cell and the angles (α, β, γ) between the vectors
d	Inter-planar spacing (d-spacing) -the perpendicular distance between adjacent parallel crystallographic planes
$\mathbf{d_0}$	Strain free inter-planar spacing
$\mathbf{d_n}$	Inter-planar spacing of planes normal to the surface
$\mathbf{d_\psi}$	Inter-planar spacing of planes at an angle ψ to the surface
E	Elastic modulus
$\mathbf{E_{hkl}}$	Elastic modulus of the diffraction plane
hkl	Miller indices describing a family of crystalline planes
n	An integer
$\mathbf{S_{1\{hkl\}}, \frac{1}{2}S_{2\{hkl\}}}$	X-ray elastic constants of the family of planes {hkl}
$\mathbf{2\theta_{\varphi\psi}}$	Peak position in the direction of the measurement
ψ (psi)	Angle between the normal of the sample and the normal of the diffracting plane
$\varepsilon_{\varphi\psi}$	Strain measured in the direction of measurement defined by the angles phi, psi
ε1, ε2, ε3	Principal strains acting in the principal directions
εx	Strain measured in the X direction
εy	Strain measured in the Y direction

University of Malaya

εz	Strain measured in the Z direction
σx	Stress in the X direction
σ1, σ2, σ3	Principal stresses acting in the principal directions
θ	Angular position of the diffraction lines according to Bragg's Law
ν	Poisson's ratio
τ	Normal shear stress
λ	Wavelength of the X-ray
ω (omega)	Angular rotation about a reference point -the angular motion of the goniometer of the diffraction instrument in the scattering plane
x, y, z	Directions relevant to Cartesian co-ordinate axis
$\langle \boldsymbol{a} \rangle, \langle \boldsymbol{c} \rangle, \langle \boldsymbol{a} + \boldsymbol{c} \rangle$	Hexagonal sub-slip systems

University of Malaya

LIST OF APPENDICES

University of Malaya

University of Malaya

CHAPTER 1: INTRODUCTION

1.1 BACKGROUND

A high demand for parts that are light with efficient structural integrity under aggressive environmental and mechanical conditions is increasing in the advanced industry. Recent demand include parts made of high strength magnesium and aluminum (Fudger, Sediako, Karandikar, & Ni, 2017). Severe plastic deformation (SPD) attracted the researchers due to its capability to produce ultra-fine grain parts; several processes are categorized under the SPD process since it was first used 2000 years ago to produce what is called Damascus Sword. Currently there are several SPD process for instance: equal channel angular extrusion (ECAE), and another method called equal channel angular pressing (ECAP), as well as high pressure torsion (HPT). (Toth & Gu, 2014). However, none of these methods was able to produce parts with tubular shape. (Ghader Faraji, Mashhadi, & Kim, 2011) introduced an innovative method named tubular channel angular pressing (TCAP). This method implements the deformation process to produce UFG parts. Which based on the occurrence of excessive dislocations due to simple shear in addition to circumferential tensile, also compressive strains as well as radial; the overall shape of the part does not change, as the main purpose is to transform its microstructure within a persistent shape (G Faraji, Mashadi, Bushroa, & Babaei, 2013). Microstructural examination using (field emission scanning electron microscopy) shows clear miniaturization in the grain size to 500 nm whereas the initial value was 150 μm. Another study on the AZ91 alloy shows a high work hardening rate during cold work associated with decreasing in elongation capability (G Faraji, Yavari, Aghdamifar, & Mashhadi, 2014). Later (M Mesbah, Faraji, & Bushroa, 2014) implemented the transmission electron microscopy (TEM) to examine commercial pure aluminum samples proceeds with TCAP and reported equiaxed grains of about

University of Malaya

310 nm that were formed after 3 passes. Several characteristics of the produced tubes has been investigated. Not match research have published in the study of residual stress in PTCAP samples. (Sanati, Reshadi, Faraji, Soltani, & Zalnezhad, 2014) Implemented Digital Shearography associated with hole drilling to inspect the through thickness residual stress in ultra-fine grain aluminum samples generated by multiple passes of SPD process and the effect of multiple passes on the residual stress. He observed that there is a reverse relationship between parallel tubular channel angular pressing (PTCAP) passes, and the values of both axial and circumferential stresses. One of the downsides of the Digital Shearography technique is the long procedures needs to address the new stress distribution between two successive increments of hole depth. Another thing is the damage that is introduced by hole drilling. WE43 magnesium alloy attracted the researcher, because of its special properties such as light weight and high strength. Furthermore, it has a hexagonal microstructure which means more likely to behave differently during SPD process. For the effect of PTCAP process on WE43 magnesium alloy and the amount of residual stress generated by the process, so far, no articles have been published before. As the majority of fatigue cracks starts on the surface, in this project we will be using XRD method to calculate the surface residual stress and the crystallite size evolution of WE43 tubular samples produced by PTCAP method. This may lead to better failure predictions.

1.2 PROBLEM STATEMENT

High residual stress and strain occurs in products that were subjected to deformation process due to the grain dislocations. This residual stress may cause cracks in parts during further deformation or during working conditions. In addition, Residual stresses have direct contribution to the product life cycle and characteristics. Considerable distortion exerted to materials, spatially for those metals with hexagonal closed packed (HCP) structure like

University of Malaya

Magnesium and Magnesium alloys, leads the part to be out of tolerance and may retard performance as a result of highly anisotropy effect. A recently developed deformation process has been introduced as previously mentioned. There is insufficient information about some of the characteristics of the parts that were produced by this process such as residual stress. While the knowledge and useful details of residual stress are desirable for the requirement of design, safety and efficiency of the produced parts.

1.3 OBJECTIVES

Based on the problem highlighted above in the problem statement, the main objectives of this research project are as below:

1. To implement X-Ray Diffraction technique to investigate the residual stress and crystallite size
2. To characterize material behavior based on residual stress, and crystallite size
3. To evaluate maximum residual stress after PTCAP.

1.4 SCOPE AND LIMITATIONS

In this project, X-Ray Diffraction was used to analyze WE43 Magnesium tubes that were processed by SPD. PTCAP method was selected as the SPD process to improve the mechanical properties of tubular parts. Approximation, Williamson Hall and $Sin^2\psi$ methods were applied to measure the material characteristics of nano-structured metals. Here are some limitations were found in this project as following:

1. Two types of stress induced by deformation process, the scope of this work is limited to the measurement after deformation process has occurred, and measurement during the deformation process is out of the scope.
2. Cutting to the tubular sample is desirable in order to fit samples in the available XRD machine. Any cut introduced to the sample may cause unreliable and deception of actual residual stress.

University of Malaya

3. X-Ray effective range is very shallow, so measurement is limited to the outer surface of the sample only.
4. X-Ray measurement is limited to the spot where the beam was exerted, not the hole part.

University of Malaya

CHAPTER 2: LITERATURE REVIEW

2.1 PLASTIC DEFORMATION

Plastic deformation introduces changes to the materials properties in different aspects; first thing observed during and after deformation is changes in shape or outer frame, while this change in shape is a reaction to the evolve of new texture and grain size, in addition, to strain and stress generated. Line defects in metals plays an important role in metal forming, and without these defects, metals are difficult to be formed. When external load applied, it causes movement of planes towards each other. This process named slip and associated with defects movement in what is generally known by dislocations. Three parameters are used to define a dislocation: its Burgers vector, dislocation density and the slip plane normal. Two types of dislocation each has different stress and strain effect screw dislocation this type has a helical path and causes the lattice to experience shear strains Figure.2.1 (b). The second type is called edge dislocation, which causes axial strains in the space lattice, Figure.2.1 (a). Regularly dislocations are a combination of the two types. An important quantity to judge the ability of material to deform is dislocation density. Dislocation density is measured as the number of emergence points through a surface. When this number is high the deformability of material is high, when it drops down material is harder to deform.

The crystal's structure plays a main role on the deformation of metals. For this reason, WE43 Mg alloy which represents hexagonal-close-packed (HCP) crystal structure was examined in this work.

University of Malaya

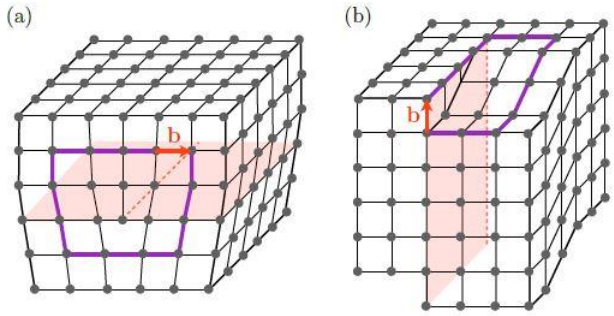

Figure 2.1:(a) edge and (b) screw dislocations in a simple cubic crystalline material, b is a Burgers vector, hatched area and dashed line illustrate the slip plane and dislocation line, respectively (Dontsova, 2013)

2.1.1 Slip

FCC metals (Aluminum), dislocations is detected on the {111} slip planes and with [110] Burgers vectors Figure (**2.4**), but with further deformation alternative planes are evolved (Kim & Jeong, 2005). The exception to this is when the [110] dislocation dissociates, or splits, into two smaller dislocations with a defect called a stacking fault between them. These partials are still on the {111} plane but have a Burgers vector in the [112] directions.

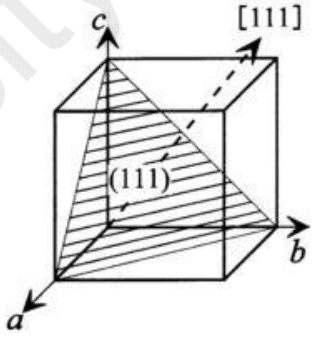

Figure 2.2: For the FCC unit cell, one of the (111) [110] slip systems (Waseda, Matsubara, & Shinoda, 2011)

Unlike the simplicity of dislocation in FCC structure, hexagonal structure is known to have more complex dislocation behavior. Three possible types of slipping direction are observed in the HCP structure: basal, prismatic and pyramidal planes, each of this plans is further classified into three basic Burgers vector types: a, c and $c + a$ (T. Ungár et al., 2007) see Figure (2.4). The ratio of the length of the unit cell in (c and a) directions c/a has a

University of Malaya

dominant effect on the preferable slip system in the material. For metals with high values of c/a, such as magnesium, limited slip systems are possible where the preferable slip plane is the basal plane (T. Simm, 2013).

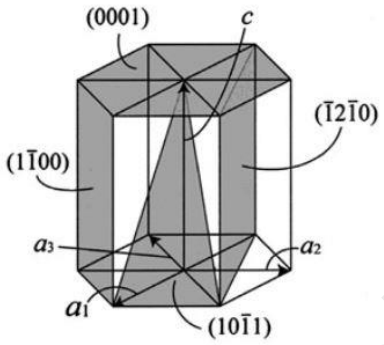

Figure 2.3: HCP representation of the a_1, a_2, a_3, c axes used, and typical planes (Waseda et al., 2011).

Slip in the $< a >$ direction is mostly preferred, but with just $< a >$ type slip it is not possible to accommodate strain in the $< c >$ direction. There are two main ways in which strain may be accommodated in the c-direction in HCP metals; $< c + a >$ slip and twinning (Dragomir & Ungár, 2002).

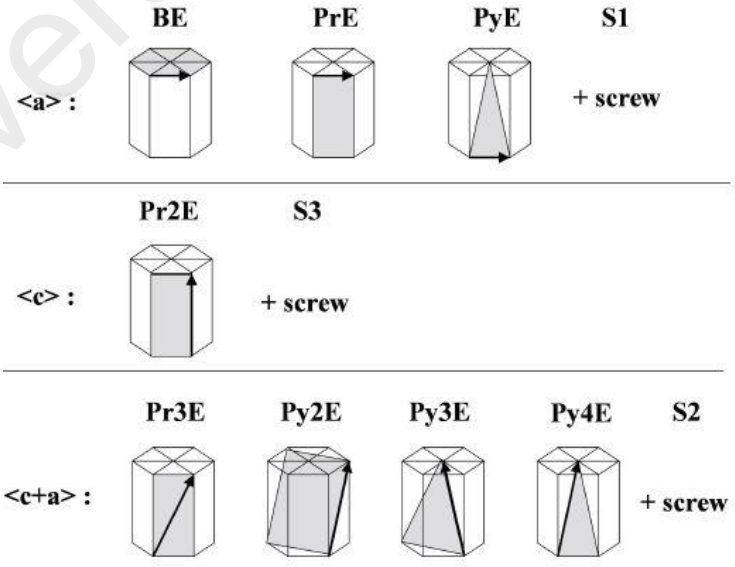

Figure 2.4: The possible dislocation slip systems in HCP (Jenő Gubicza, 2014).

University of Malaya

2.1.2 Twinning and Stacking Faults

Usually the easiest way to respond to a deformation process is by slip. While in those metals that have a few slipping planes such in hexagonal structure then twinning is most likely to occur as a response to the deformation process. In general, twinning is favored at high strain rates and low temperatures (Zhu, 2006). The important role of twinning in plastic deformation is that it causes changes in plane orientation so that further slip can occur. Stacking faults can be produced during plastic deformation and play an important role in deformation. A stacking fault is a planar fault, which causes the organized rearrangement of the position of atoms from the perfect crystal structure.

2.2 TCAP MICRO-STRUCTURE FORMATION

Severe plastic deformation has been widely used to produce ultra-fine grain sized as this kind of structure is known to enhance the metal material properties. SPD process has the advantages over other strengthening methods that grain size refinement dose reduce sample toughness. (Azushima et al., 2008). Ultra-fine grains produced by the PTCAP is a result of imposing high strain and shear level to the material without changing the tube size, because of that several passes can be repeated to reach optimum re-crystallization. As in all SPD techniques, after the first pass the grain refinement reach a high level at which dislocation density at its maximum and decreases when proceeding with higher number of passes (Barmouz, Abrinia, & Khosravi, 2013). Existence of high density of dislocations increase the possibility of producing UFG materials and influence the yield strength. Thus, increase in the number of passes improve the refinement by a small amount comparing to the firs pass (G Faraji et al., 2014), because of the decreases in added dislocation intensity. (J Gubicza, Chinh, Krállics, Schiller, & Ungár, 2006) justified the decrease of dislocations by the relation between strain and dislocations, when strain reaches a high level this causes

University of Malaya

saturation in dislocation density. (Koizumi & Kuroda, 2018) reported continuous increases of the high angle grain boundaries associated with the cumulative passes until successfully generate homogeneous nanostructures. we must be aware of the fact that TEM gives a microscopic local value for the dislocations in inhomogeneous samples (HajyAkbary, Sietsma, Böttger, & Santofimia, 2015). (M Mesbah et al., 2014) referred this phenomenon to the fact that TEM device cannot distinguish the grain boundaries if the grains have not been clearly transformed from elongated to equiaxed grains. On the other hand (Balogh, Capolungo, & Tomé, 2012) proofed the superiority of XRD measurement over TEM to identify dislocations and sub-grains from the coherent diffraction domain in SPD materials.

2.3 RESIDUAL STRESS

Mechanical stresses that is measured after the external load has removed or machining has been completed is named Residual stresses, because these kind of stresses do not vanish, after the load is no longer being exist; in some references they refer to this phenomenon as the internal stress (Singh & Agrawal, 2015). Stress is self-equilibrating, where different types of stress contributes in different direction to the overall state of the material, summation of this forces equals to zero and named equilibrium. This has the advantages to make the material stable. However, it introduces bending momentum inside material. If this momentum is extremely high, releasing part of this stress by cut might causes the parts to be deflected. Most of the machining and deformation processes causes additional residual stresses. Additional, stresses might also evolve because of inhomogeneous strains during the loading service of the product. Such as: temperatures, pressure, high strain rates thereby creating residual stresses. For the situation that the stress measurement is taking by the time the material is subjected to the load, is out of the scope. The residual stress backed inside the material act as high energy reservoir, this energy might be released by crack generation,

University of Malaya

crack spreading and may impact performance or causes the shape to be changed. However, residual stresses are not always unfavorable to the material characteristics. Residual stresses can be classified in to two main types, compressive ($\sigma < 0$) and shear residual stress ($\sigma > 0$). Product application determines whether the existence of stress is favorable or not. Compressive residual stress for example increases the Fatigue resistance. In addition, it reduces erosion cracking. Consequently, existence of such properties is an added advantageous for any parts to be used in aggressive environments. On the other hand, shear residual stress increases stress cracking risk (Huber & Heerens, 2008).

Another approach classified residual stresses into three types based on the length scale of influence. Type I also referred to as "macro" residual stresses this type usually appears in machined parts as a result of inhomogeneous distribution of strains, and has a long range of effect, often calculated using finite elements. Type II and III referred to as "micro" residual stress that varies in the micron range. Type III are residual stresses that is associated with plastic deformation this type acts over the atomic dimension, for example, dislocations and point defects (Schajer, 2013). Although we mentioned some explanations for each type of residual stresses, in real life, components have all the residual stress types due to nonmechanical influences.

2.4 STRUCTURAL CHARACTERIZATION

First attempt to measure residual stress, methods with the intervention of cutting process was used. This method named after the material behavior as deflection methods, or according the stress behavior as relaxation methods. in general, this approach is known as destructive methods, because it damages small or large part of the sample being measured. Some parts are expensive or hard to be machined and cut without introducing extra stress and heat during the cut. Researchers start to look for other methods that do not required any

University of Malaya

machining to get accurate results to save the measured product. This approach became popular and known as non-destructive methods. A part of these methods is qualitative such as Thermoplastic and indentation test and others are quantitative. Some of these methods are more sophisticated and more accurate than others but has limitations, we referred to (Schajer, 2013) for detailed information about them. Among the quantitative methods X-ray diffraction (XRD) is non-destructive method and capable to address UFG materials and structural properties at the same time. Measuring residual stress with X-ray diffraction is described as an indirect method, it based on the stress *vs* strain relation in Hook's low, lattice strain can be measured directly by the X-ray as we may assume a linear elastic shafting of the crystal lattice plane. To be more specific, in the current project materials that is processed by SPD, strain is mainly caused by dislocations, this strain is expressed as broadening of X-ray line profiles where we get the reading from (J Gubicza et al., 2006), then by implementing the young's modulus we get the residual stress. In general X-ray is a useful method to calculate near surface stresses, because of the shallow penetration of the X-ray to the sample. Any attempts to calculate farther thickness than the penetration distance, removal of layers is required to provide access for the x-ray into the aimed thickness. The X-ray penetration varies according to the grain size, type of radiation, incident angle and beam size. Since the measurement depends on the incidence beam location and grain size the change of location may result in different values. Previous researchers used complementary methods to verify their results such as destructive methods (Brown et al., 2011) or finite elements analysis (Reyes-Ruiz et al., 2016).

2.4.1 Challenges and Limitations

In case of holloed cylinders, we may need to have access into the inner surface of the cylinder. Machining processes may add extra surface residual stresses into the sample that

University of Malaya

is being prepared for inspection. In such cases where sectioning is necessary, then this should be accomplished using Electro Discharge Machining (EDM) to avoid introducing significant residual stress, caution is necessary when cutting or avoided if possible, as it can raise the sample temperature, this might vanish the residual stresses (Fitzpatrick et al., 2005). Several approaches were introduced by the previous researchers to accommodate the sectioning relaxations. (Brown et al., 2011) used deflection method, as a cut were made along the axial axis of the cylinder. That cut results of two sections, therefore each section with a "c" shape. Observation was made to estimate the change of the circumference diameter as an indicator of momentum released. In case this method is used, one has to be aware that residual stresses measured by XRD were taken from a specific location, where on the other hand, residual stress that is obtained from the sectioning is not. Another thing, XRD is able to measure the actual stress while sectioning measures the released stress only (Béchade, Toualbi, Bosonnet, Castelnau, & de Carlan, 2013). (Nico Hempel, Nitschke-Pagel, & Dilger, 2016) Did the XRD measurement to a cylindrical sample on the outside surface before and after cutting and recorded the difference, if any. Additionally, laser triangulation used to monitor the radial deformation on the outer surface. (N Hempel, Nitschke-Pagel, & Dilger, 2014) implanted strain gauges during the cutting process to detect any variations during or after sample cutting, besides repeating the XRD measurement before and after. Through thickness residual stress can be addressed by layer removal. This material removal requires chemical attack to avoid additional stress by conventional methods.

Round samples can be treated as a flat sample, as long as the X-ray beam spot size is small enough. Hoop direction measurement requires a maximum spot size of $R/4$, and $R/2$ for

University of Malaya

axial measurements, where R is the radius of curvature of the sample (Fitzpatrick et al., 2005).

This device has the challenge of converting measured lattice strains. strain is produced by the summation of information from every crystal along the lattice column that is perpendicular to the incident, and reflected X-ray plane into the components of the stress tensor (Miller & Dawson, 2014). The reflection depends on the orientation distribution function of the sample. SPD process divide crystallite into smaller components; this causes difficulties in the interpretation of gathered information form the diffracted beam pattern that has low intensity and large broadening. Therefore, it needs more attention when interpreting the results.

X-ray theory behind the measurement of the type I is based on the determination of the accurate spacing between crystallographic planes. Inaccurate results might take place in case we could not identify the type II stress as it has similar to the type I effect. To distinguishe between these two types we may use either deflections methods, or multiple exposure of X-ray (Kesavan Nair & Vasudevan, 1995). Further explanation for the second technique can be found in (Schajer, 2013)

2.4.2 $\mathbf{Sin^2\,\psi}$ Method

The XRD technique is based on the change of a diffracted plane position, which corresponds to a change in interplanar spacing d that is caused by deformation process. Bragg's equation $n\lambda = 2d\sin\theta$ is used to detect the d changes. Elastic strain ε in case of material deformation is defined as the change in the interplanar spacing from their strain-free value $\varepsilon = \Delta d/d_0$ of crystals inside material. Accordingly, it is necessary to have an

University of Malaya

accurate measure of d_0, the stress free spacing. The strain results can then be converted into stress following Hook's low (Withers & Bhadeshia, 2001).

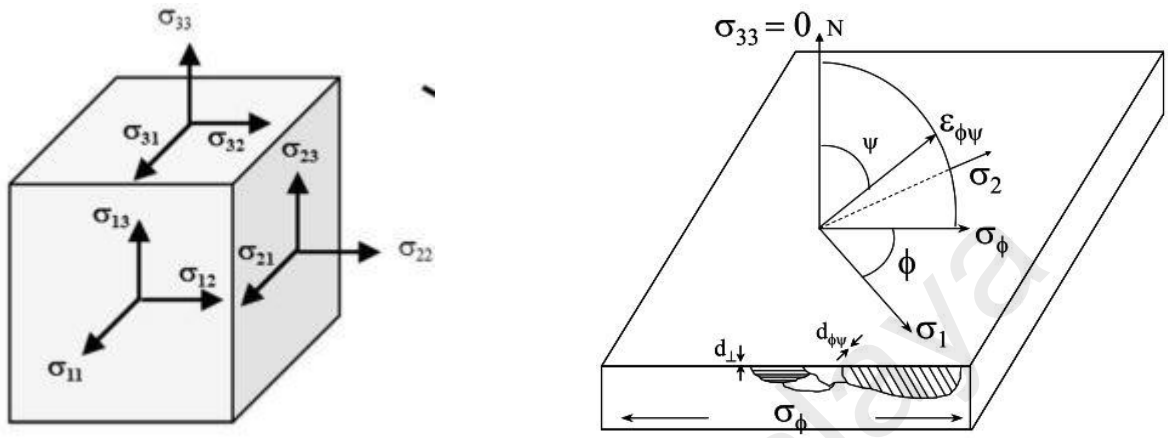

Figure 2.5: Schematic showing Stresses acting on an elemental unit cube to the left, and to the right the act of diffraction on the plane surface (Fitzpatrick et al., 2005)

X-rays penetrates only thin surface layer; small depth of penetration means that the sampled region can often be assumed to be in plane stress. To determine an in-plane biaxial plane stress (σ_{11}=σ_{22}, σ_{33}= 0) only the in-plane strain ε_{11} or the out of-plane strain ε_{33} is required.

$$\sigma_{11} = \frac{E\,\varepsilon_{11}}{1-v} \quad OR \quad \sigma_{11} = -\frac{E\,\varepsilon_{33}}{2v} \tag{1}$$

If the material is considered isotropic then biaxial strain is represented by Eq. (2)

$$\varepsilon = \frac{d_\psi - d_0}{d_0} = \left(\frac{1+v}{E}\right)\sigma_{11}\sin^2\psi + \left(\frac{2v}{E}\right)\sigma_{11} \tag{2}$$

Measurements are made at different psi ψ tilts, then, the inter-planar spacing is plotted, or 2θ peak position versus $\sin^2\psi$ as an inclined line with intersect. After that, the gradient of the line is calculated. This assumes a zero stress at $d_0 = d_n$, where d_0 is the intercept of the y-axis when $\sin^2\psi = 0$. With knowledge of the Poisson ratio $v = 0.27$ and Youngs modulus $E = 44\ GPa$ of the measured material, the stress can then be calculated from such plot by:

University of Malaya

$$\sigma = \left(\frac{E}{1+v}\right) m \qquad (3)$$

Where m is the gradient of the d vs. $\sin^2\psi$ line, negative and positive slopes correspond to compressive stress and tensile stress respectively. This equation gives an average value of the residual stress within the shallow layer penetrated by the X-ray beam. One advantage of this principle is the fact that no standard free strain sample is required, since d_0 can be substituted in Eq. (2) as previously explained without significant error, because elastic strains are typically less than 1%, so that $d_0 \cong d_{\psi=0}$ (Withers, Preuss, Steuwer, & Pang, 2007);(Pamnani et al., 2015). Another method to determine d_0 by (Birkholz, 2006) is to calculate the strain free tilt ψ^* by equation $\sin\psi^* = \sqrt{\frac{2v}{1+v}}$.

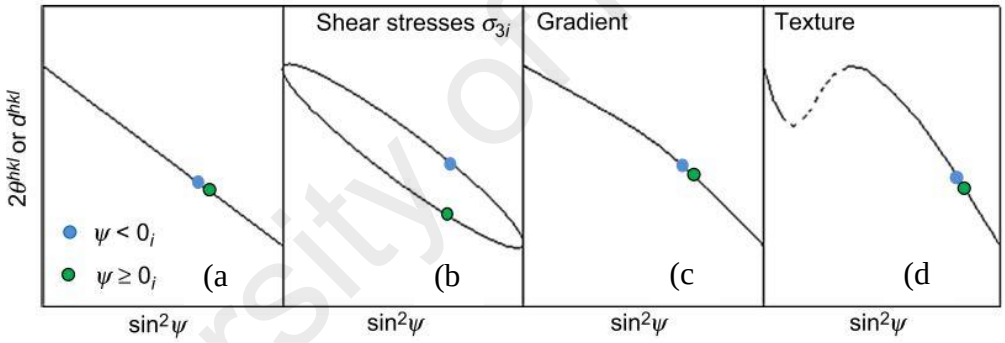

Figure 2.6: Different types of $sin^2\psi$ distributions depending on the investigated material (Epp, 2016)

However, Eq. (2) assumes a linear relation between d and $\sin^2\psi$ in isotropic materials, Whereas, $\sin^2\psi$ curves tend to have scattering or shapes as presented in Fig.**2.6**. This is due to the anisotropy of the material, insufficient knowledge of the diffraction elastic constants, crystallographic texture, broader diffraction peaks with low intensity, shear stress, non-spherical grain, and inhomogeneous strain (Kapoor, Lahiri, Padmaprabu, & Sanyal, 2002);(Jeong et al., 2015). Anisotropic system has different properties in different directions mostly present in solid (crystalline) materials (Pecharsky & Zavalij, 2008).

University of Malaya

Splitting Curve shape in box named (b), is a result of shear-stress in direction σ_{31}/σ_{32}. The $\sin^2\psi$ curve will show a typical ψ-splitting due to asymmetric strain distribution in negative and positive ψ tilting. Measurement has to be taken in positive and negative ψ angles to consider this variation. Graph (c) is a result of either a gradient residual stress within the effective depth of the X-ray or the material was deformed plastically. Graph (d), shows a wavering distribution this represents an inhomogeneous residual stress state in the different direction, because of highly textured material. For the nonlinear graph (c) and (d), the standard $\sin^2\psi$ method is not applicable and more advance method with nontrivial calculations has to be implemented for stress calculation (Epp, 2016).

2.4.3 Line Broadening

Metals that was subjected to deformation process experience micro structure imperfections, because of the planar defects. Line broadening (LB) has been used to get microstructural information about the material from the profile shape and expansion of Bragg reflections such as crystallite size and strain. Later it became more specific to get detailed information like distribution of dislocations. Generally, two important aspects of the XRD profile, the profile shape and the peak width. The width of a peak profile can be described by different parameters which are commonly used for the calculation of the size-strain broadening (Scardi, Leoni, & Delhez, 2004). The most popular, integral breadth (IB) and full width at half maximum (FWHM) are used to express peak width. FWHM is the simplest, and often used when other methods are not possible, either because the quality of the diffraction peak is low or there is a limited number of diffraction peaks available. However, researchers have criticized FWHM of the broadening profile line to give untrustworthy approximation therefore, the IB is recommended to be used (Bushroa, Rahbari, Masjuki, & Muhamad, 2012).

University of Malaya

Perfect crystals according to the dynamical diffraction theory causes extremely sharp profile, in which no broadening effect occurred but that is caused by the principle limitations. However, crystal imperfections in materials, will introduce broadening associated with the Bragg peak that results from faultless crystal diffraction. Crystallite size is a measure of the size of a coherently diffracting domain. Because of the existence crystallite size is smaller than particle size, in fact particles are made of crystallite. Strain in crystallite is classified into two types based on its distribution. Uniform strain "homogeneous" also referred to as ''micro-strain' and non-uniform strain "inhomogeneous". Uniform strain rises because of changes in the unit cell size and effect in anisotropic way that means it has different value when measured in different directions. This leads to a change in the actual inter planner spacing d_0 and peak shafting. Homogeneous strain is a result of crystallite imperfections, (stacking faults, twin boundaries, and antiphase boundaries), this type does not cause profile broadening (Tamás Ungár, Balogh, & Ribárik, 2010). Non-uniform strain leads to change in atoms location and to peak broadening. This kind of strain is caused by point defects, vacancies, site-disorder, plastic deformation, and poor crystallinity. Hence the strain that exist in ultra-fine grains has an impact on the crystallite size measurement. It is confirmed that the profile broadening has a direct relation with lattice strain and inverse relation with crystallite size. Information about the strain introduced by grain refinement is necessary for the fully comprehension of size measurements and to achieve clear image on the modifications that was introduced to the material properties. Up to this point we only covered part of the broadening effects this part is named physical factors. Separation of the physical broadening components can be accomplished if the diffraction angle known. Another part from the experimental broadening, which alter the separation process is a broadening

University of Malaya

caused by instrumental factors such as inherited depression of $K_{\alpha 1}$ and $K_{\alpha 2}$, and the specifications of the x-ray instrument's optics. Therefore, correction is essential to substitute the instrumental broadening before proceeding to the separation (Savaloni, Gholipour-Shahraki, & Player, 2006). More or less reliable approaches exist to study the components that contributes to the line broadening, two approaches are widely being in used convolution and de-convolution approaches. De-convolution approach define the instrumental effect by either investigating a standard sample with negligible structural line broadening; the detected broadening is then accepted to be the instrumental broadening, or more recently, by using instrument with pre-defined instrumental/geometrical details of the diffraction pattern; then this broadening is subtracted from the original shape (Mittemeijer & Welzel, 2008). On the other hand, instrumental broadening in a convolution approach is added instead. (Zhang, Zhou, & Lavernia, 2003) stated that the broadening factors can be addressed based on the assumptions that the original and instrumental broadening can be approximated according to Cauchy (Lorentz) or Gaussian shape profile functions, a combination of these functions are listed below:

$$\beta_{exp} = \beta + \beta_{ins} \quad \text{(CC)} \quad (4)$$

$$\beta_{exp}^2 = \beta^2 + \beta_{ins}^2 \quad \text{(GG)} \quad (5)$$

$$\frac{\beta}{\beta_{exp}} = 1 - \left(\frac{\beta_{ins}}{\beta_{exp}}\right)^2 \quad \text{(CG) voigt} \quad (6)$$

where $\beta_{exp}, \beta,$ and β_{ins} are the integral breadth of experimental broadening, physical broadening, and instrumental broadening, respectively.

2.4.3.1 Williamson Hall

Scherrer method (Scherrer, 1918) is known to be the first implementation to the line broadening in crystallite size identification. The theory behind Scherrer method states that

University of Malaya

the broadening of peak at half of its height B is inversely proportional to the crystallite size. Later (Wilson, 1963) redefined it to be β "integral breadth apparent size". Apparent size represents the distribution of crystallite columns in various length. Difficulties appears when trying to use a constant shape factor K to represent crystallite shape, while crystallite do not have a constant shape or size. Scherrer's method under-estimates the crystallite size, because it assumed that the brooding is a result of the size factor only and ignored other factors that contribute to the broadening such as micro-strain or residual stress type III (Venkateswarlu, Chandra Bose, & Rameshbabu, 2010). The values produced by Scherrer equation is not very accurate and mostly used to get primary value before proceeding to more complex methods.

As we discussed earlier line broadening is caused by a combination of multiple effects. This fact is reflected by Williamson Hall method (WH), which basically combines the Scherrer equation with the effect of strain broadening. Strain causes broadening as a result of crystal faultiness and distortion is related by $\varepsilon = \beta_s/\tan\theta$ (Khorsand Zak, Abd. Majid, Abrishami, & Yousefi, 2011). It is worth to mention that β is the integral breadth in radian. Separation of size and strain broadening that occurs at the same time is possible by considering the peak width as a function of 2θ, depending on explicit assumptions as to the shape of the peak profile caused by each effect (Zhang et al., 2003). As the peak profile takes bell-shaped functions, it is often approximated as Cauchy or Gaussian functions, look equations (4), (5), (6).(Edwards, 1975) suggested that the Gaussian function is more likely to represent the strain effect, whereas the broadening that is caused by size effect tends to follow Cauchy's profile. To eliminate the effect of the instrumental broadening it is necessary to identify its profile broadening by standard material before we conduct the experiment, then subtract it from the measured samples.

University of Malaya

$$\beta_{hkl} = \beta_{size} + \beta_{strain} \quad (7)$$

$$\beta_{hkl} = \left(\frac{k\lambda}{D\cos\theta}\right) + \varepsilon \sin\theta \quad (8)$$

Rearranging Eq. (8) we get:

$$\beta_{hkl}\cos\theta = \frac{k\lambda}{D} + 4\varepsilon\sin\theta \rightarrow Y = b + aX \quad (9)$$

It is necessary to plot equation (9) in order to obtain the slope where we get the strain and intercept to calculate grain size Figure (**2.7**). Dislocation density can be calculated using $\rho = \frac{2\sqrt{3\varepsilon}}{Db}$ where b is the magnitude of burgers vector (Koizumi & Kuroda, 2018). One should be aware of the fact that for material that is build-up by small crystallite, produce profile better to be represented as Lognormal or Gamma distribution, in this case the previous assumption of Cauchy and Gaussian function is no more valid. Profile produced by dislocations is not valid for such assumption as well. Failure to choose appropriate profile function to represent each property or to select the related peaks may lead to misleading, because this will be reflected as high standard deviation value "scattered data".

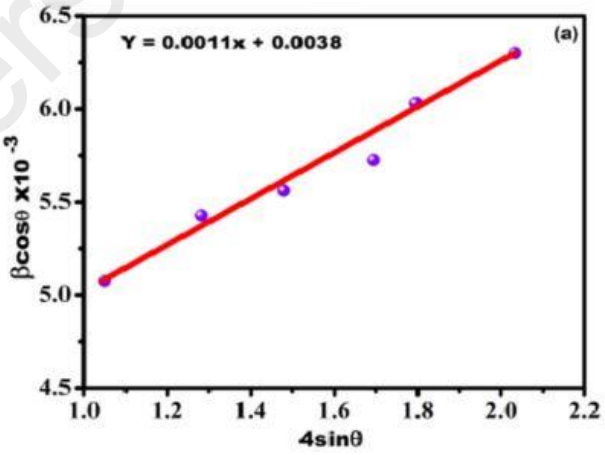

Figure 2.7: The WH of RuO2 NPs sample (Sivakami, Dhanuskodi, & Karvembu, 2016)

The size obtained by classical WH is criticized to include effects due to stacking faults and dislocations. To adapt with the scattering caused by dislocations and other parameters such

University of Malaya

as planner defects (Scardi et al., 2004), and anisotropy which is not considered in conventional WH (Chandekar & Kant, 2018), several modified WH equation was proposed. Most popular are uniform stress deformation model (USDM) (10), uniform deformation energy density model (UDEDM) (11) and size strain plot method (SSP) (12). All the mentioned methods do not consider the anisotropy. Another modification was introduced to adapt with this parameter will be discussed later.

$$\beta_{hkl}\cos\theta = \frac{k\lambda}{D} + \left(\frac{4\sigma\ sin\,\theta}{E_{hkl}}\right) \tag{10}$$

$$\beta_{hkl}\cos\theta = \frac{k\lambda}{D} + \left(4\sin\theta\ \left(\frac{2u}{Y_{hk;}}\right)^{1/2}\right) \tag{11}$$

$$d_{hkl}\beta_{hkl}\cos\theta = \frac{K}{Dv}\left(d_{hkl}^2\beta_{hkl}\cos\theta\right) + (\varepsilon/2)^2 \tag{12}$$

(Sivakami et al., 2016) inspected RuO2 nanoparticles by plotting the XRD data using the whole approaches mentioned above, he found that of the SSP model is more precise than other methods, as the line is fitted more accurately, with less scattering points. (Khorsand Zak et al., 2011) used the same approaches and recommended SSP method in case of isotropic line broadening, as it has advantage over the rest models, because not much weight is given to the higher angle reflections.

2.4.3.2 Warren-Averbach

A limitation of the classical Williamson-Hall method according to Warren-Averbach (WA) method (Warren, 1969) is that strain direction dependent effect is not considered. Has an advantage over WH method that no pre-assumption of size strain shape function is required in case of WA, Because of that WA is the most accurate method but requires much effort than other methods. The main idea behind size-strain separation in WA method is the difference dependency of size-strain broadening on the order of reflection (this method was

University of Malaya

developed originally for plastically deformed metals). size-strain analyses in WA based on Fourier method. (McKeehan & Warren, 1953) states that the Fourier coefficients for pure physical curve shape A_n are the multiplication of the size coefficient A_L^S which depends on the column length from this we can get information about distribution of crystallite size (Pourghahramani & Forssberg, 2006), and the strain coefficient A_L^D which depends on domain distortion. The coefficients are numerically calculated ignoring faults effect (Marinkovic, Avillez, Saavedra, & Assunção, 2001).

$$A_L = A_L^S A_L^D \tag{13}$$

Referring to (McKeehan & Warren, 1953) coefficients in eq.(13) separated to get equation approximated bellow:

$$\ln A_L = \ln A_L^S - 2\pi^2 \langle \varepsilon_k^2 \rangle L^2 K^2 \tag{14}$$

Where $K^2 = h_0^2/a^2$, $h_0^2 = h^2 + k^2 + l^2$, a is latest constant, L is the displacement of two cells in column which equals to:

$$L = \frac{n\lambda}{2(\sin\theta_2 - \sin\theta_1)} \tag{15}$$

where each peak is measured between θ_1 and θ_2 Bragg angle interval which means the angles that correspond to the initial and final angle of the diffraction peak considered, n is n^{th} neighbor in the same column starting from zero. Therefore, if $\ln A_L$ is plotted versus h_0^2 for different values of L, the intercept at $h_0^2 = 0$ directly gives the size coefficient, $\ln A_n^S(L)$, and the slope will give the value of mean square averaged strain, $\langle \varepsilon_k^2 \rangle$ for each value of L.

After size coefficient are obtained using eq. (14), (Warren, 1969) shows that the intercept of the initial slope gives the surface weighted domain size. crystallite size, D_s, and that the surface weighted crystallite sizes distribution, $P_s(L)$:

University of Malaya

$$\left[\frac{dA_A^S}{d\,L}\right]_{L\to 0} = \frac{-1}{D_s} \tag{16}$$

$$P_s(L) \propto \frac{d^2 A_n^S(L)}{d\,L^2} \tag{17}$$

Where $\propto$ represent the stacking fault probability.

Warren-Averbach method requires at least two orders of reflections along each crystallographic direction (family) and when higher order reflections are weak and difficult to analyze Williamson-Hall method is employed (Maniammal, Madhu, & Biju, 2017) (Sivakami et al., 2016)

2.4.3.3 Modified Williamson Hall And Modified Warren-Averbach Method

Difficulties appear when analyzing plastically deformed materials, because of the anisotropic broadening. In case where the anisotropy is mainly caused by dislocation, another modification to WH method is suggested where the contrast factor C plays the main factor to eliminate scattering that is caused by anisotropy effect (T. H. Simm, Withers, & Quinta da Fonseca, 2016). It is also applicable to materials with mono-crystalline and high textured effect (Robert W. Cheary, C.C. Tang, P.A. Lynch, M.A. Roberts, 2001).The contrast factor is a function of the elastic constants of the material and the vectors defining the dislocation. When this factor is introduced to WH method equation can be written as in equation (18) and (19)

$$\beta_{hkl} = \frac{0.9}{D} + f_M k(\rho\overline{C_{hkl}})^{1/2} \qquad \text{MWH1} \tag{18}$$

$$\beta_{hkl} = \frac{0.9}{D} + f_M^2 k^2(\rho\overline{C_{hkl}}) \qquad \text{MWH2} \tag{19}$$

Where $\Delta K = \beta_{hkl} = total\ integral\ bredth\ (better)\ or\ FWHM$ $f_M^2 = \left(\frac{\pi R^2 b^2}{2}\right)$, $k = \frac{2\sin\theta}{\lambda}$,

University of Malaya

The values of $\overline{C_{hkl}}$ can be obtained by relatively long equations as in (T. Ungár, Dragomir, Révész, & Borbély, 1999). With an assumption of equally populated slip systems, the mathematical equation can be rewritten in simplified form for cubic structure (T. Ungár & Tichy, 1999). In HCP metals where more possible slip systems, the contrast factor is simplified as in (Dragomir & Ungár, 2002).

$$\bar{C} = \overline{C_{h00}}\,(1 - qH^2) \qquad \text{FCC} \qquad (20)$$

$$\bar{C} = \overline{C_{hk0}}\,(1 + q_1 x + q_2 x^2) \text{ where} \qquad \text{HCP} \qquad (21)$$

In this work, to avoid the long contrast factor calculation procedures in HCP metallic structure, where many slip systems contribute to the calculations. Two choices for the contrast factor calculation are available. Either to use the calculated Contrast factors for HCP popular materials in (Dragomir & Ungár, 2002), or to be generated through a program called ANIZC, which is available online at http://metal.elte.hu/anizc/. ANIZC was developed by (Borbély, Dragomir-Cernatescu, Ribárik, & Ungár, 2003). Elastic constants inputs $C_{11}, C_{12}, C_{13}, C_{33}, C_{44}\ and\ c/a$ required for the program, for popular materials is available in (Tromans, 2011). For the WE43 alloy is $C_{11} = 63.5\ GPa$, $C_{12} = 24.85\ GPa$, $C_{13} = 20\ GPa$, $C_{33} = 66\ GPa$, $C_{44} = 19.3\ GPa$ and $a = 0.64\ nm$, $b = 2.22\ nm$, $c = 0.52\ nm$, $c/a = 0.815$ (Gao et al., 2012), (Jiang et al., 2017).By plotting $\Delta K = \beta_{hkl}$ against $K\bar{C}^{1/2}$ as shown in figure **2.8** the intercept and slope of the plot give the grain size and the product of $f_M^2\rho$ respectively.

University of Malaya

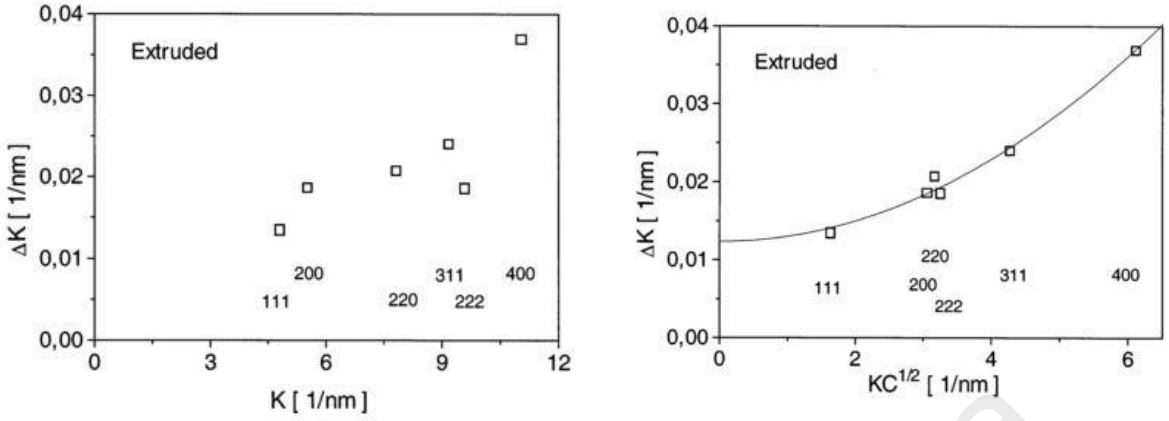

Figure 2.8: To the left classical Williamson–Hall plot , and modified Williamson–Hall plot to the right both of them for a sample deformed by ECA (T. Ungár, Gubicza, Hanák, & Alexandrov, 2001)

WA method has been modified to be known as modified Warren Averbech (MWA). Basically, it follows the conventional WA with the consideration of Contrast factor. Where the mean square strain is written as a function of the contrast factor as follows:

$$\langle \varepsilon_k^2 \rangle = \left[\frac{\rho \bar{C} b^2}{4\pi}\right] \ln(R_e/L) \qquad (22)$$

Then substitute in the main WA Eq.14

This method is used to obtain details about the dislocation structure. This method is known to be long and exhausting. In addition, the long procedures may contain errors due to separation of each effect in each stage. Therefore, MWH provide a good approximation to calculate the size strain with anisotropy effect (T. H. Simm et al., 2016).

2.4.3.4 Approximation Method

Approximation method is a method that uses line broadening profile to calculate grain size and strain. this method is often overlooked. It was first explored by (Umansky, Skakov, Ivanov, & Rastorguev, 1982). The main idea behind this method is to draw a graphical

University of Malaya

relation between two integral breadth of XRD peaks at θ_1 and θ_2 from the graph we get some values to substitute in Scherrer equation to get grain size and Williamson to get strain. WA method usually experience difficulties to identify weak and high order reflections (Maniammal et al., 2017). These errors are not significant in Approximation method. Thus, Approximation method might be a good replacement to WA, because they have similar trend as both of them results in larger value than those calculated by Scherrer formula. Approximation method was utilized to separate size-strain effect of TiSiN thin film instead of Warren-Averbach and briefly explained by (Bushroa et al., 2012) as follows.

$$\frac{m_1}{\beta_1} = \frac{1}{2}\left[1 - 4\frac{n_1}{\beta_1} + \sqrt{1 + 8\left(\frac{n_1}{\beta_1}\right)}\right] \tag{23}$$

$$\frac{\beta_2}{\beta_1} = \frac{\{[V(m_1/\beta_1)] + [2(n_1/\beta_1)]W\}^2}{\{[V(m_1/\beta_1)] + [4(n_1/\beta_1)]W\}} \tag{24}$$

$$V = \frac{m_2}{m_1} = \frac{\cos\theta_2}{\cos\theta_1} \tag{25}$$

$$W = \frac{n_2}{n_1} = \frac{\tan\theta_1}{\tan\theta_2} \tag{26}$$

$$\frac{n_2}{\beta_2} = \frac{n_1}{\beta_1} \times \frac{W}{\beta_2/\beta_1} \tag{27}$$

After the X-Ray graph is created, the most significant two beaks and that has similar plane family is taken and the associated angles are named θ_1 and θ_2 respectively. Assuming that m_i represents the broadening due to grain size effect only at each peak and n_i represents broadening caused by strain only at each peak. β_1, β_2 are the total broadening for peak one and two in radian, from the previous assumptions it is obvious that the ratio of strain broadening to the overall broadening n_1/β_1 varies between 0-1. Substituting these values in Eq. 23. Then values obtained from this equation are used to get β_2/β_1 from Eq.24. A graph is plotted between m_1/β_1 and β_2/β_1. Another graph is drawn between n_2/β_2 and β_2/β_1

University of Malaya

using Eq.27. see Figure.2.9. After the two graphs has been plotted, experimental value of $(\beta_2/\beta_1)_{Exp}$ that is obtained from the original X-ray graph is reflected into the graph drawn to get the experimental values of $(n_2/\beta_2)_{Exp}$ and $(m_1/\beta_1)_{Exp}$. $(m_1)_{Exp}$, $(n_1)_{Exp}$are obtained from the graph and substituted in Scherrer equation $D = \frac{K\lambda}{m_1 \cos\theta_1}$ to get grain size and Williamson $\varepsilon = \frac{n_2}{4\tan\theta_2}$ to get strain. This method is applicable only if the following conditions were satisfied: 0 < (m_1/β_1) or (m_2/β_2), and (n_1/β_1) or (n_2/β_2) < 1.

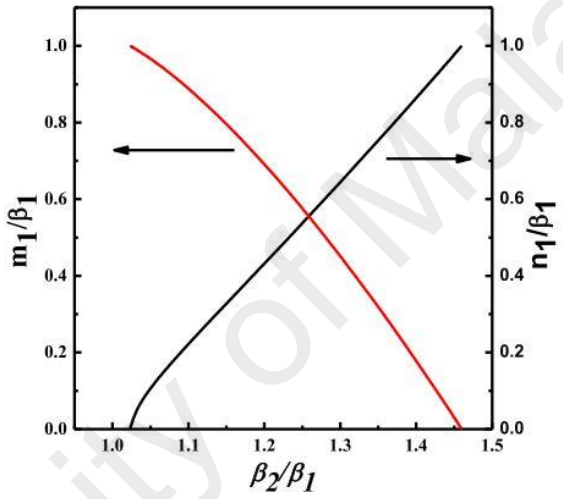

Figure 2.9: A plot of $(m_1/\beta_1)\ and\ (n_1/\beta_1)\ versus\ (\beta_2/\beta_2)$ (Bekri, Shaalan, & Ahmed, 2015)

University of Malaya

CHAPTER 3: MATERIALS AND METHODS

In order to accomplish the objectives of this project successfully, there must be accurate and feasible methodology and appropriate materials. In this chapter, the methods and materials have been selected to achieve the objectives based on reliable previous research papers. Initially the sample materials were prepared by another researcher, followed by X-ray Diffraction. Detailed information is elaborated respectively as below.

3.1 MATERIALS

Deformation process effects materials structure differently according to the material property, grain size and elastic constants. In addition, the material itself can have certain applications that other materials are not as good to be used instead, such as weight and level of toxicity inside human body. For those reasons, a special Magnesium alloy WE43 was used in this experiment to show how advanced alloy with HCP structure are affected by TCAP deformation process.

Table 3.1 Components of WE43 alloy.

Elements	Content (%)
Magnesium (Mg)	Remainder
Yttrium, (Y)	3.7-4.3
Zirconium, (Zr)	0.4
Neodymium (Nd)	2.4-4.4

3.1.1 Sample Preparation

WE43 Magnesium alloy tubes were used for this experiment. Thanks to Mr. Mohsen as the samples was prepared by him as follows: a cylindrical tube with a dimension of $50\ mm$ in length, outer diameter of $20\ mm$ with a wall thickness equals to $2.5\ mm$; these tubes were

University of Malaya

subjected to deformation process that is called TCAP up to 3 passes, one forward shot, and one backward shot together are considered to be one cycle (pass). The process was conducted in high temperature up to 300 °C. This process was originally invented to change the internal structure of the metal without changing the overall shape; in order to enhance the mechanical properties of the tube.

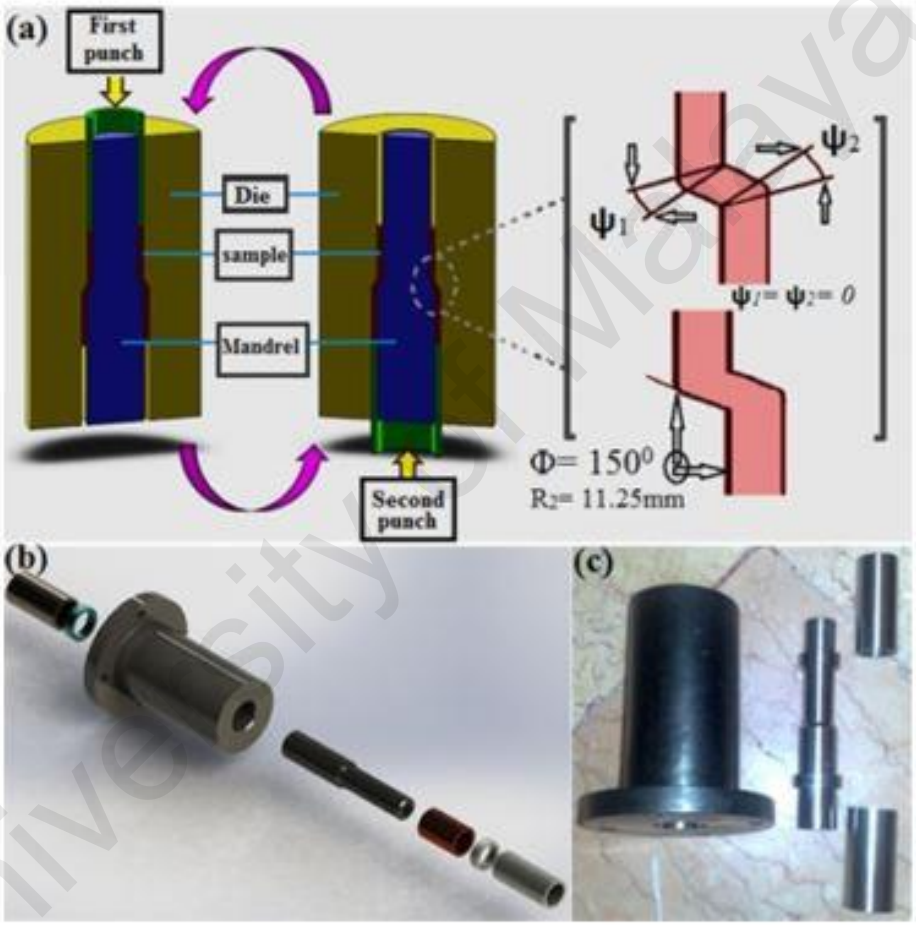

Figure 3.1 schematic diagram of the deformation process (Mohsen Mesbah et al., 2016)

3.2 DIFFRACTION MEASUREMENTS (XRD)

Lattice parameters were measured using X-ray powder diffraction on the axial direction for the as-received (pre-ECAP) condition and after 1, 2, and 3 passes. Measurements were only conducted on the outer surface. Inner tubes surface was not inspected, sectioning was

University of Malaya

necessary to fit samples inside the available XRD machine. A square of $10 \times 10\ mm$ was cut from the edge of the tube by Diamond cutter (EDM cutting is preferred).

Figure 3.2 Demonstration to the way the samples was cut

3.2.1 Experimental X-Ray Setup

The PANalytical's X'Pert instrument machine has been applied to do the experimental measurement. CuKα radiation with $\lambda = 1.54056$ Å, parallel beam setup was implemented to provide good measurement independent of the alignment condition and to reduce errors that is introduced by non-flat samples (Vermeulen, 2006). The generator voltage and current were 45 kV and 40 mA. The scan range was set to $2\theta = 5 - 90$, 2θ step was set at $0.026°$ and counting time per step was 50 s to provide good and fine intensity. Constant omega Ω angle was employed and a computer generated different ψ angles automatically by means of this relation $\psi = \theta - \Omega$, as shown in Figure 3.3. The residual stress evaluation was accomplished by the $\sin^2 \psi$ technique, in which diffraction peak that has a well-shaped high-intensity single diffraction peak, i.e. not significantly overlapped was selected (Q. Luo & Jones, 2010), unlike conventional XRD that requires high angle usually $2\theta > 125$, new equipment that is equipped with Parallel Collimators is able to observe residual stress at low 2Theta angles as low as $2\theta > 30 - 40$, where it is easier to get perfect peak shapes in this range (Vermeulen, 2006). The high angle requirements are compulsory for the goniometers that are sensitive to alignment errors only. In this work the selected peak was

University of Malaya

$2\theta = 69$. Instrumental profile correction was considered as default, because only one XRD machine is connected to the computer. Unlike the situation where more than one machine is connected to the same computer; standard LaB6 powder samples has to be measured and saved on the software program before proceeding with profile analysis. This standard simple is usually provided by NIST. Afterward, the grain size, strain and dislocation density, were observed using Williamson– Hall and Approximation method.

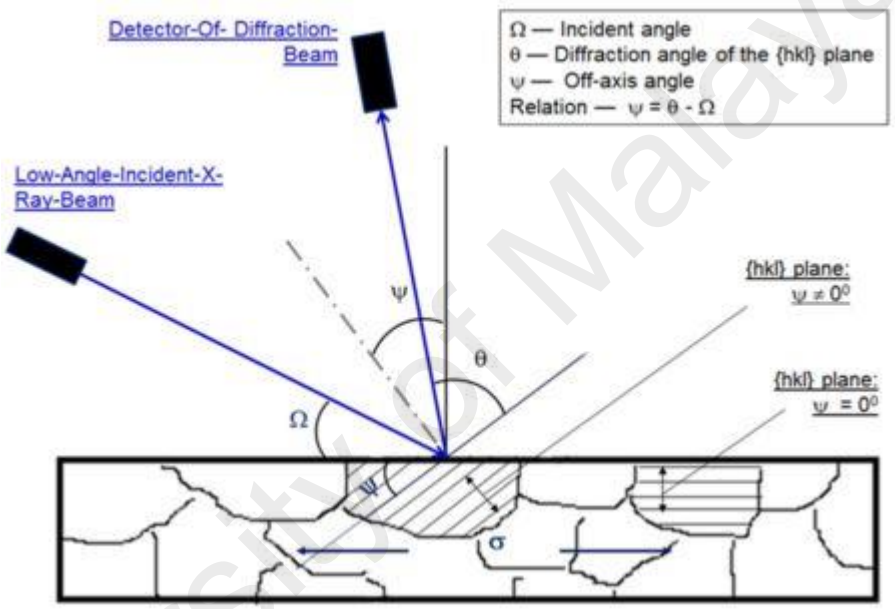

Figure 3.3 XRD Geometric set-up for the purpose of residual stress measurements (Quanshun Luo & Yang, 2017).

University of Malaya

CHAPTER 4: RESULTS & DISCUSSION

4.1 X-RAY DIFFRACTION

In this chapter, the results were obtained by conducting an XRD scanning based on reliable methodology. In fact, initially the X-ray diffraction result was attained as shown below in figure 4.1. It can be observed that the absolute scan for WE43 samples with three passes started from S_0 as received and ended at S_3. These graphs were used as a source to extract information about the material being observed. These graphs were used to understand and analyze the residual stress, strain and crystallite size. Special XRD software and methods were used for further analysis.

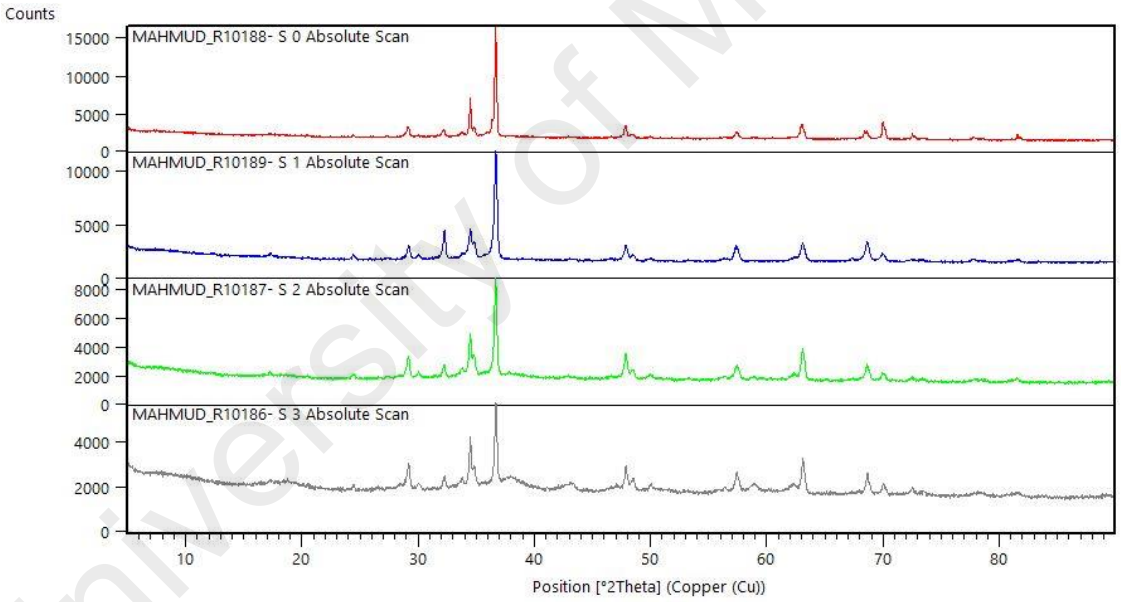

Figure 4.1 XRD patterns of WE43 samples, S_0 as received, S_1 one pass, S_2 two passes and S_3 three passes.

4.2 RESIDUAL STRESS ANALYSIS

Philips Xpert Highscore software was used to accomplish a multi-steps treatment for the raw XRD graph, to extract required data for the residual stress analysis. First of all, we run

University of Malaya

the XRD inspection on a wide range of 2Thet angle, this step is known as Absolute scan. The second step is to choose the best peak within the range we mentioned before $2\theta > 40$, this peak will be used in the second scan. The second scan is mainly used for the residual stress analysis where several scans to the same peak with different ψ angles are generated to inspect the d-spacing. The multiple scans are shown in Figure 4.2.

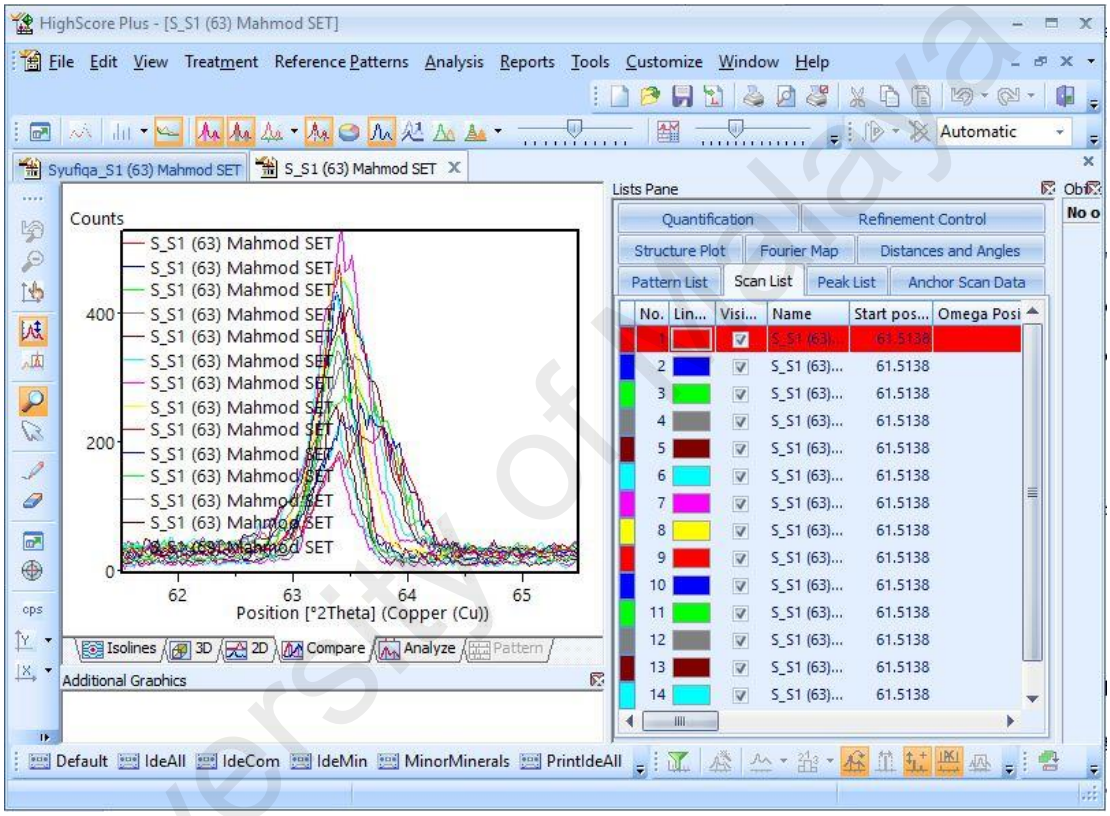

Figure 4.2 Residual stress scan results

Each peak was treated individually. The treatment includes: background termination, peak identification, removal of kα-2 peak, and peak profile fitting using Person VII. The fitted peak appears in a blue line while the raw peak in orange figure 4.3.

University of Malaya

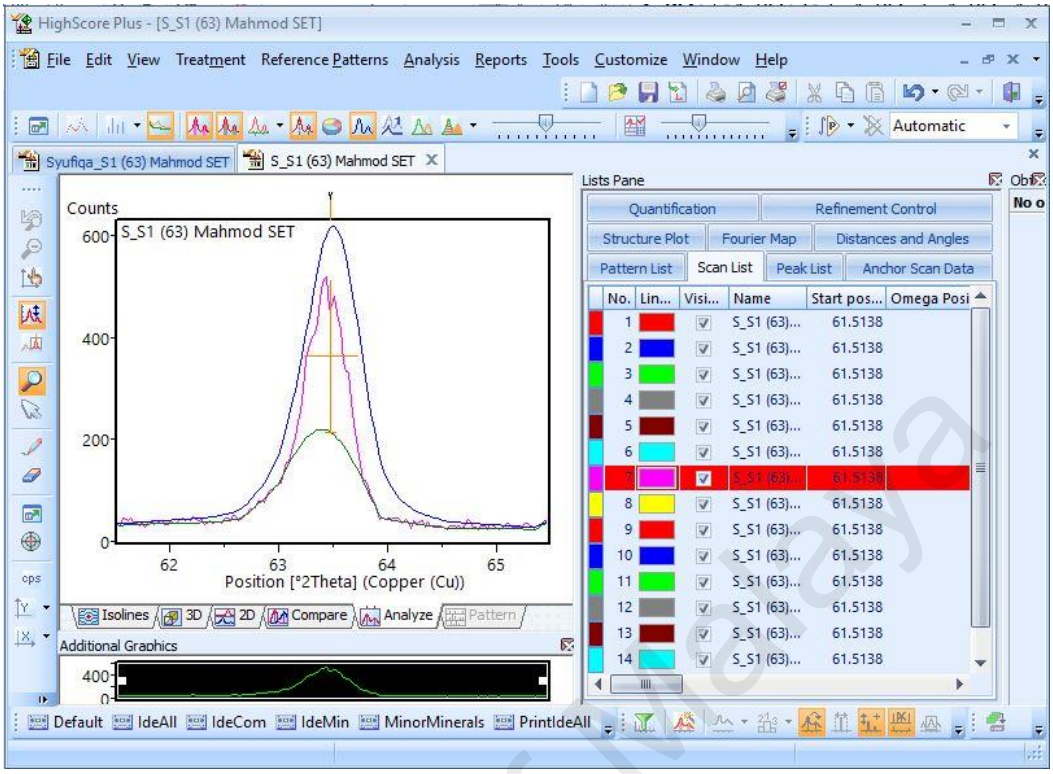

Figure 4.3 Individual peak after fitting

This profile fitting is aimed to recalculate the mid-point and to correct the shape of the remaining kα-1 peak, because each peak of the raw XRD graph is actually a combination of two different wavelengths kα-1 and kα-2. These two wavelengths may appear in three different shapes: two distinct peaks as in (A), one blended peak (D) or partially separated peaks as in (B and C). These two peaks have to be separated in all cases.

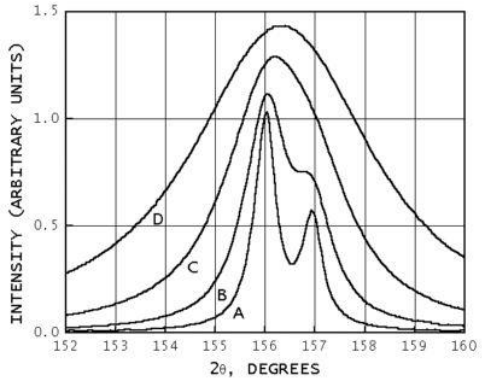

Figure 4.4 Different shapes of kα-1 and kα-2 peaks shapes (Prevéy, 1986)

University of Malaya

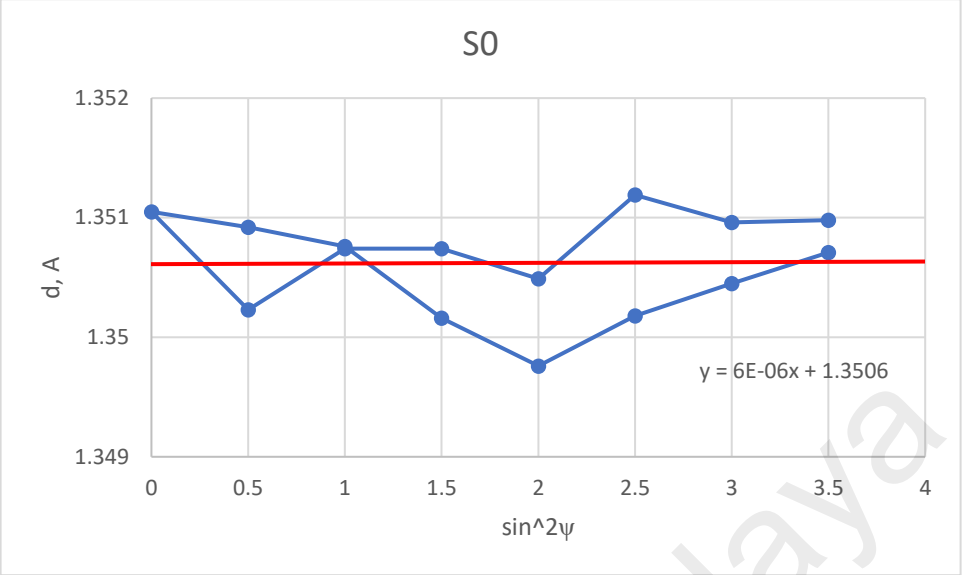

Figure 4.5 d-spacing versus $\sin^2\psi$ plot for zero passes

To obtain residual stress y-axis in the above graph has to be converted from d-spacing into strain by $\frac{d_n - d_0}{d_0}$ where d_0 is the value of d-spacing at $\sin^2\psi = 0$. Then, substitute the slope value of a least square line in Eq.3 in order to get residual stress value.

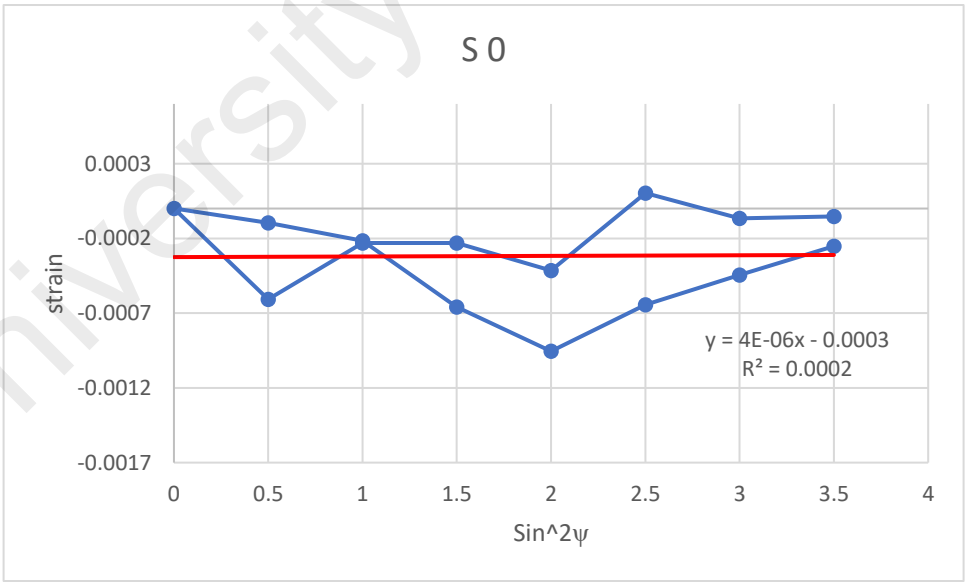

Figure 4.6 strain versus $\sin^2\psi$ residual stress determination

University of Malaya

Residual stress values for each sample are shown in table 4.1

$$\sigma = \left(\frac{E}{1+v}\right) m$$

$$\sigma = \left(\frac{44}{1+0.27}\right) 4 \times 10^{-6} = 1.3 \times 10^{-4}\ MPa$$

Table 4.1 Residual stress values for the S_0, S_1, S_2, S_3 Samples

Sample	Residual stress value in (MPa)
S_0	1.3×10^{-4}
S_1	-2.77×10^{-4}
S_2	-6.929×10^{-4}
S_3	-6.929×10^{-4}

4.3 WILLIAMSON HALL

For all the line broadening analysis, absolute XRD scan has to be run through 2θ interval between 5° to 90°. Larger angles are avoided as peaks at higher angles are not suitable for line profile analysis. After the row data has been produced, profile refinement was conducted for peaks identification purpose, then profile fitting was implemented by assigning polynomial function to the background and Pseudo Voigt function to profile refinement. Background removal and $K_{\alpha 2}$ stripping was only implemented after the profile fitting has done successfully, because the program calculates the overall parameters and take them into consideration during the profile fitting process. Once the final outcomes are available then we implement them in the rest of the calculations.

University of Malaya

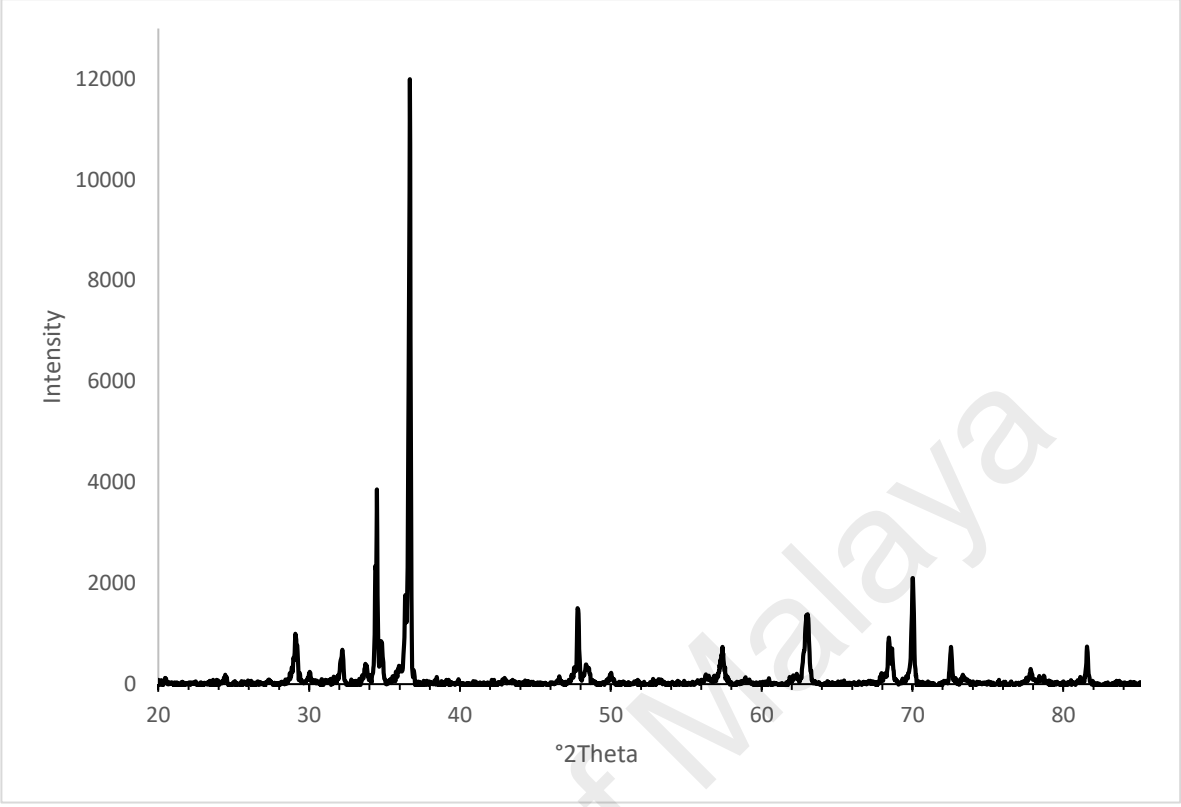

Figure 4.7 XRD profile of S_0 sample after refinement process

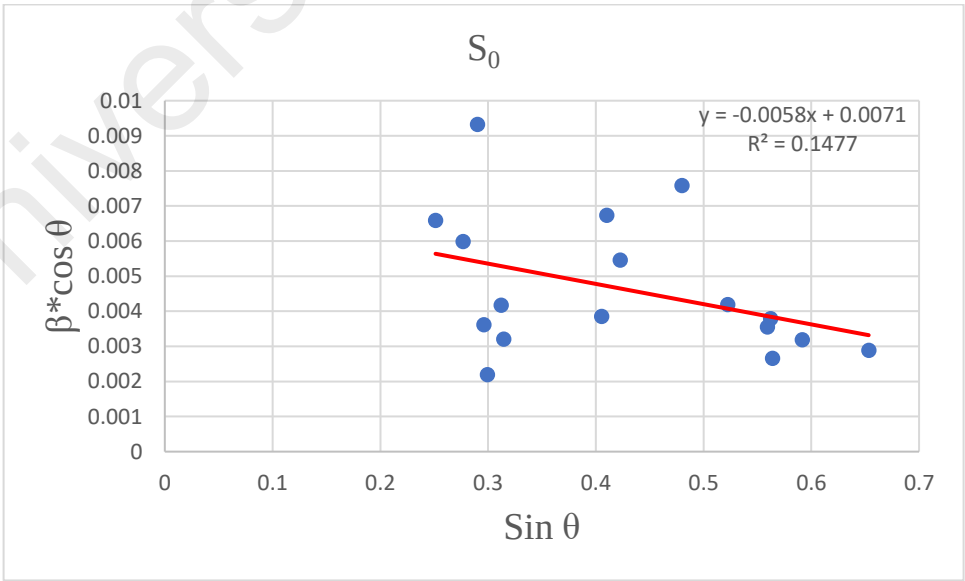

Figure 4.8 Conventional Williamson Hall plot for (S_0) sample

University of Malaya

By implementing equation (8) the grain size and strain can be calculated directly Grain size calculation is as follows:

$$\frac{k\lambda}{D} = intersection\ value$$

$$\frac{0.94 * 1.54056\ \text{Å}}{D} = 0.0071\ \text{Å}$$

$$D = \ 203.96 \times 10^{-1} = 20.39\ nm$$

Strain does not need any further calculation, as it equals to the slope value.

Table 4.2 Results of Williamson Hall method

Sample	Grain size (nm)	Lattice strain
S0	20.39	-1.45×10^{-3}
S1	19.30	9.25×10^{-4}
S2	21.29	1.45×10^{-3}
S3	14.33	2.73×10^{-3}

4.4 APPROXIMATION METHOD

In the approximation method, once the integral breadth values of the XRD peaks has been gathered. Two peaks were chosen provided the distance between them is reasonable. Where the contribution of size and strain broadening being different to get good values. In this calculation the chosen beaks were $\theta_1 = \ 36.64°$, $\theta_2 = \ 63.06°$ more information about the associated broadening of each peak in each pass is provided in table **4.3**. After that, experimental value of integral breadth $(\beta_2/\beta_1)exp$ was extended, from the corresponding value on X-axis to the graph, then reflected from the graph to y-axis. This process was repeated on Fig 4.9 to get (m) values and on Fig4.10 to get (n) values, where β_1 and β_2 are known. Finally, Scherrer $D = \frac{K\lambda}{m_1 \cos\theta_1}$, and Williamson equation $\varepsilon = \frac{n_2}{4\tan\theta_2}$ was implemented to get the grain size and strain respectively.

University of Malaya

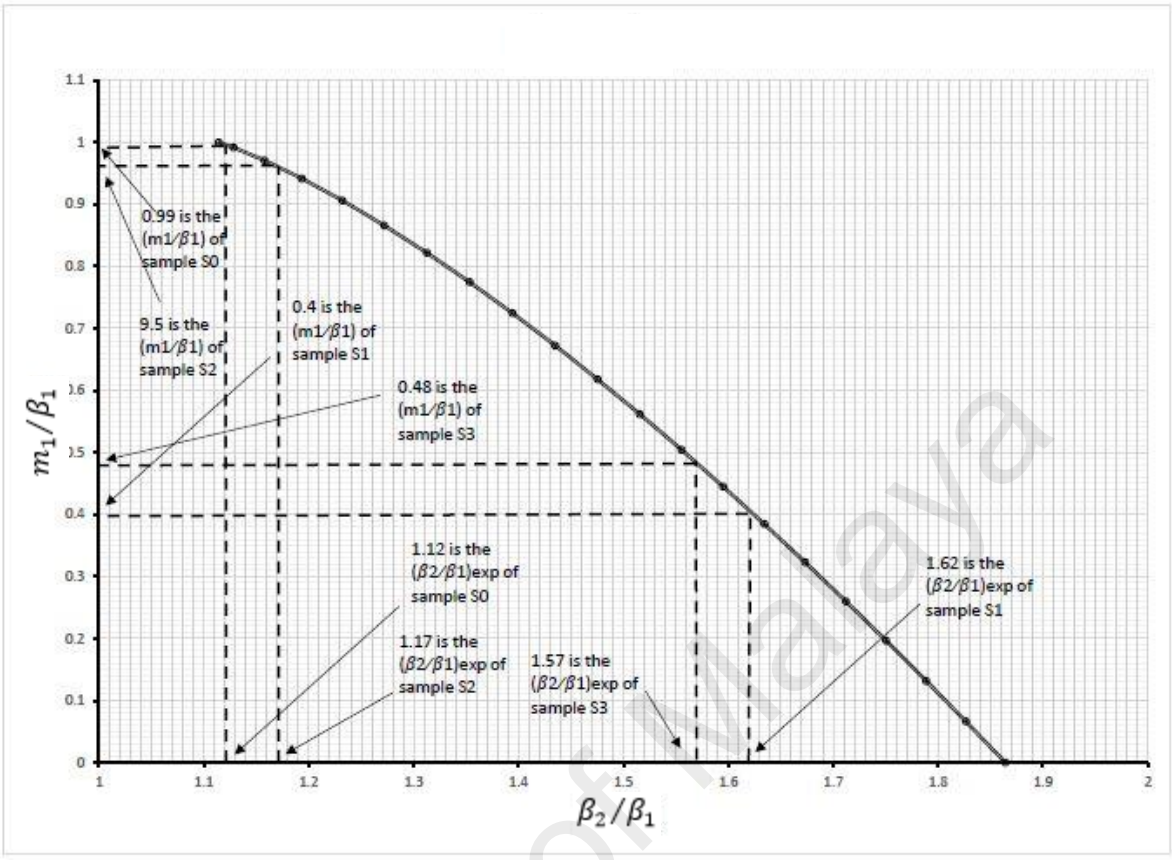

Figure 4.9 Plot of β_2/β_1 versus m_1/β_1

Detailed calculations that was used to draw the curves are available in the Appendix

University of Malaya

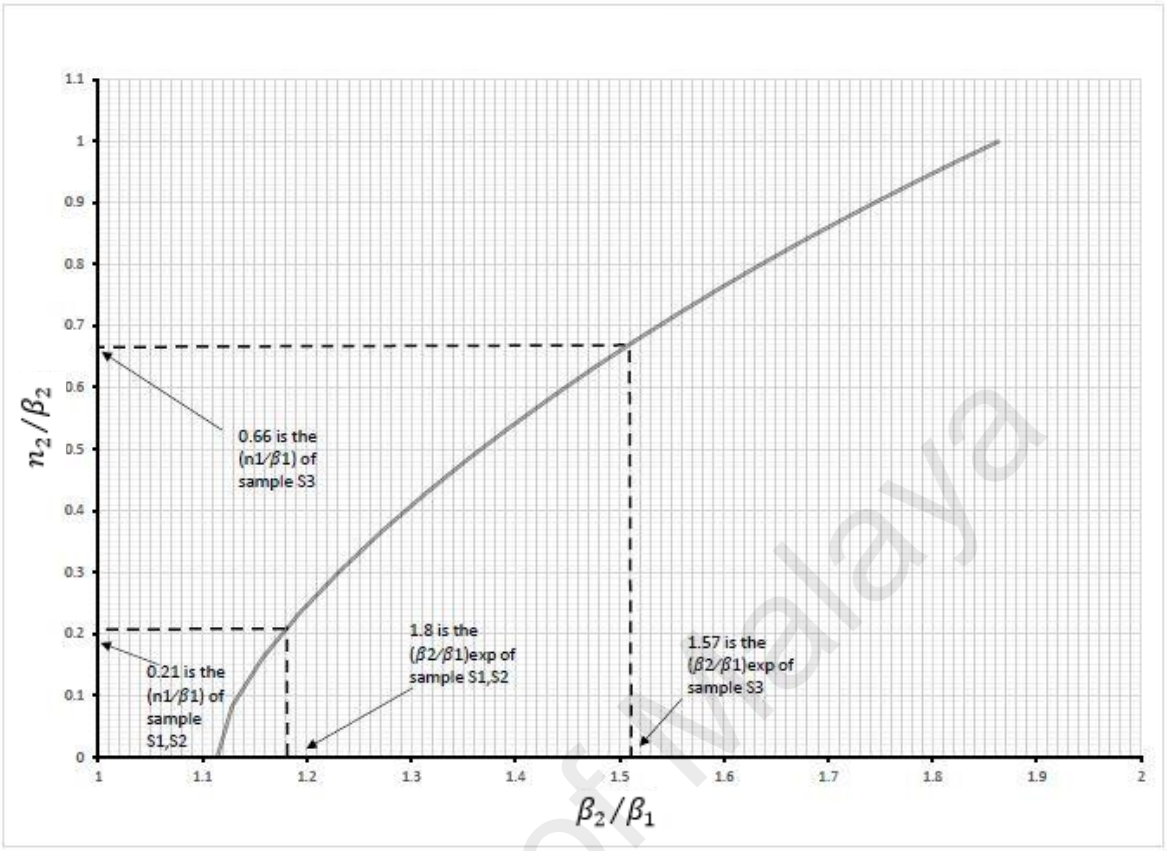

Figure 4.10 Plot of β_2/β_1 versus n_2/β_2

Table 4.3 The implemented values and outcomes of Approximation method.

Sample	β_1 (Radian)	β_2 (Radian)	β_2/β_1	m_1/β_1 exp	n_2/β_2 exp	m $\times 10^{-3}$	n $\times 10^{-3}$	Grain Size nm	Strain
S_0	0.0043824	0.2812	1.12	0.99	—	4.34	—	35.25	—
S_1	0.008449017	0.8119	1.63	0.4	0.21	3.38	1.77	45.26	7.22×10^{-4}
S_2	0.008449017	0.5709	1.18	0.95	0.21	8.02	1.77	19.07	7.22×10^{-4}
S_3	0.006975924	0.6025	1.51	0.48	0.66	3.34	4.6	45.8	1.87×10^{-3}

University of Malaya

DISCUSSION

Raw XRD data shows no significant difference in peaks intensities as well as no significant shafting except for the graph of third pass for the reason of the very small scale of the outcomes. However, this fact does not mean that no changes has introduced to the characteristics of the observed tubes. HighScore plus software is one of the best XRD software that is reliable and recognized among the world-wide organization was implemented to get accurate results among the small variations. In general, the experiment was designed to make observation on one spot of the outer surface of each sample. This might has led to systematic error. As to get reliable and accurate results, the experiment should have designed to make several observations along the tube and around the circumference. This is significant procedure to average the outcomes. In the current results, some variance was observed due to the fact that XRD result was taken from one spot only. More details about the outcomes and comparison between different methods are elaborated below.

4.5 RESIDUAL STRESS

Residual stress calculation on axial axis was conducted by $\sin^2 \psi$ method. This calculation was processed by the positive and negative ψ tilts. This particular setting was used to detect and compensates the effect of shear stress. Parallel beam technology was also considered to minimize the error that is caused by non-straight surface effect of the sample. Splitting of the $\sin^2 \psi$ curve was observed which indicates the presence of shear residual stress effect or non-uniform distribution of stress within the observed location. This was consistence with the FEM simulation on Abaqus. Simulation shows significant variation of residual stress inside the deformed tubes. This variation results from different exposure to deformation process in different areas and thickness. The extreme edge of the tube for

University of Malaya

example was not exposed to deformation as same as the amount of deformation exposed to the middle or first edge of the tube. Residual stress that was measured by $\sin^2\psi$ method shows obvious change from positive value (tensile) before the first PTCAP pass to negative residual stress value (compressive). This is consistent with (Sanati et al., 2014) findings, as he mentioned that compressive stress was dominant at the surface of the tubes after PTCAP process, because of the friction between the tube surface and die. The negative stress values increased as the number of pass increases. However, the residual stress did not show any change after the second pass where the second and third pass got exact same values. Constant residual stress after the second pass might be referred to the saturation of dislocation density. Furthermore, cyclic heating and cooling process between the deformation cycles contribute to the amount of stress being added and released by the heating process when external load is applied, this phenomenon was explained by (Kwak & Hwang, 2018).

4.6 APPROXIMATION METHOD VS WILLIAMSON HALL

Two different methods were utilized to measure the lattice strain and crystallite size. To start with, the value of strain in the zero pass was left planked, because of the fact that Approximation method is only valid for the positive values. Where the β_2/β_1 was located out of the graph. Hence, cannot be calculated. For the rest of the strain values calculated by Approximation method has shown rabidly decreased while crystallite size shows some variation. On the other hand, Williamson hall method shows decreasing in the crystallite size and variation in the lattice strain values. The main different between the two method is that crystallite size calculated by Approximation method has higher values than of those calculated by Williamson Hall which is in consistence of the literature where it is stated that Approximation method always shows higher crystallite size value.

University of Malaya

Table 4.4 Comparison table between Approximation and Williamson hall method

Sample	Crystallite size (nm)		Lattice strain	
	WH	Approximation	WH	Approximation
S_0	20.39	35.25	-1.45×10^{-3}	—
S_1	19.30	45.26	9.25×10^{-4}	7.22×10^{-4}
S_2	21.29	19.07	1.45×10^{-3}	7.22×10^{-4}
S_3	14.33	45.8	2.73×10^{-3}	1.87×10^{-3}

4.7 MATERIAL PROPERTY

From the results we can confirm that PTCAP deformation process produces better parts; where the deformation process refines the crystallite size. Grains in polycrystalline materials made up of crystallite. Therefore, grain size must have decreased as will. Smaller grain size has a direct impact on material density, therapy parts are stronger. The friction between the part and die during the process produced a compressive stress on the outer layer of the tubes. Compressive stress on the surface is favorable, because the tube acquired additional wear resistance.

University of Malaya

CHAPTER 6: CONCLUSION

PTCAP process is a branch of sever plastic deformation process that was developed to enhance tubular parts. The effect of this process on magnesium alloy properties was investigated by means of XRD. It was found that the crystallite size decreases with the increase of the pass number. The microstructure evolution caused the residual stress on the part to change from tensile to compressive stress. As a result of the compressive stress on the surface and the smaller crystallite structure, the strength and durability of the processed part was enhanced, where it can withstand more wear and tear. From the comparison between WH and Approximation method one can get to the conclusion that the results of WH method was closer to the expectation as the crystallite shows reduction in size while the results shows oscillation in case of Approximation method. For these reasons, Approximation method is easy and accurate enough to get a first impression, but not when accurate values are very important.

Some recommendations to be mentioned for future wok are listed here: More observation point along and around the tubular part surface is recommended to average the overall stress, strain and crystallite size. One observation on each sample is not the best practice where some variation of stress on the part surface is more likely to exist. In case through thickness observation by means of XRD is required, chemical reaction is the best method to remove the outer surface layer by layer, after that XRD values has to be corrected mathematically. Finally, advanced XRD models like modified Williamson Hall for better address the microstructure and strain evolution this might support the current results. Also, to execute 3D FEM simulation with the intention to obtain accurate outcomes with the minimum effort.

University of Malaya

REFRENCES

Azushima, A., Kopp, R., Korhonen, A., Yang, D. Y., Micari, F., Lahoti, G. D., … Yanagida, A. (2008). Severe plastic deformation (SPD) processes for metals. *CIRP Annals*, *57*(2), 716–735. https://doi.org/10.1016/j.cirp.2008.09.005

Balogh, L., Capolungo, L., & Tomé, C. N. (2012). On the measure of dislocation densities from diffraction line profiles: A comparison with discrete dislocation methods. *Acta Materialia*, *60*(4), 1467–1477. https://doi.org/10.1016/j.actamat.2011.10.037

Barmouz, M., Abrinia, K., & Khosravi, J. (2013). Using hardness measurement for dislocation densities determination in FSPed metal in order to evaluation of strain rate effect on the tensile behavior. *Materials Science and Engineering A*, *559*, 917–919. https://doi.org/10.1016/j.msea.2012.08.086

Béchade, J. L., Toualbi, L., Bosonnet, S., Castelnau, O., & de Carlan, Y. (2013). Macroscopic and Microscopic Determinations of Residual Stresses in Thin Oxide Dispersion Strengthened Steel Tubes. *Materials Science Forum*, *768–769*, 296–303. https://doi.org/10.4028/www.scientific.net/MSF.768-769.296

Bekri, M., Shaalan, N. M., & Ahmed, A. S. (2015). Thermal evaporated WO3 nanoparticles film under different evaporation pressures for NO2 sensing. *Digest Journal of Nanomaterials and Biostructures*, *10*(2), 603–613.

Birkholz, M. (2006). *Thin Film Analysis by X-ray*. *Book*. https://doi.org/10.1002/3527607595

Borbély, A., Dragomir-Cernatescu, J., Ribárik, G., & Ungár, T. (2003). Computer program

University of Malaya

ANIZC for the calculation of diffraction contrast factors of dislocations in elastically anisotropic cubic, hexagonal and trigonal crystals. *Journal of Applied Crystallography*, *36*(1), 160–162. https://doi.org/10.1107/S0021889802021581

Brown, D. W., Holden, T. M., Clausen, B., Prime, M. B., Sisneros, T. A., Swenson, H., & Vaja, J. (2011). Critical comparison of two independent measurements of residual stress in an electron-beam welded uranium cylinder: Neutron diffraction and the contour method. *Acta Materialia*, *59*(3), 864–873. https://doi.org/10.1016/j.actamat.2010.09.022

Bushroa, A. R., Rahbari, R. G., Masjuki, H. H., & Muhamad, M. R. (2012). Approximation of crystallite size and microstrain via XRD line broadening analysis in TiSiN thin films. *Vacuum*. https://doi.org/10.1016/j.vacuum.2011.10.011

Chandekar, K. V., & Kant, K. M. (2018). Size-strain analysis and elastic properties of CoFe 2 O 4 nanoplatelets by hydrothermal method. *Journal of Molecular Structure*, *1154*, 418–427. https://doi.org/10.1016/j.molstruc.2017.09.104

Dragomir, I. C., & Ungár, T. (2002). Contrast factors of dislocations in the hexagonal crystal system. *Journal of Applied Crystallography*, *35*(5), 556–564. https://doi.org/10.1107/S0021889802009536

Edwards, A. J. (1975). HP Klug and LE Alexander, x-ray diffraction procedures for polycrystalline and amorphous materials: Wiley-Interscience, New York, 2nd edn., 1974, xxv+ 966 pp. price£ 18.55. Elsevier.

Epp, J. (2016). 4 - X-ray diffraction (XRD) techniques for materials characterization. In *Materials Characterization Using Nondestructive Evaluation (NDE) Methods* (pp. 81–124). Woodhead Publishing. https://doi.org/10.1016/B978-0-08-100040-3.00004-3

University of Malaya

Faraji, G., Mashadi, M., Bushroa, A., & Babaei, A. (2013). TEM analysis and determination of dislocation densities in nanostructured copper tube produced via parallel tubular channel angular pressing process. *Materials Science and Engineering A*, *563*, 193–198. https://doi.org/10.1016/j.msea.2012.11.065

Faraji, G., Mashhadi, M. M., & Kim, H. S. (2011). Tubular channel angular pressing (TCAP) as a novel severe plastic deformation method for cylindrical tubes. *Materials Letters*, *65*(19–20), 3009–3012. https://doi.org/10.1016/j.matlet.2011.06.039

Faraji, G., Yavari, P., Aghdamifar, S., & Mashhadi, M. (2014). Mechanical and Microstructural Properties of Ultra-fine Grained AZ91 Magnesium Alloy Tubes Processed via Multi Pass Tubular Channel Angular Pressing (TCAP). *Journal of Materials Science and Technology*, *30*(2), 134–138. https://doi.org/10.1016/j.jmst.2013.08.010

Fitzpatrick, M., Fry, A., Holdway, P., Kandil, F., Shackleton, J., & Suominen, L. (2005). Determination of Residual Stresses by X-ray Diffraction - Issue 2. *Measurement Good Practice Guide*, (52), 74. https://doi.org/10.1007/s00028-005-0194-y

Fudger, S., Sediako, D., Karandikar, P., & Ni, C. (2017). Residual stress induced mechanical property enhancement in steel encapsulated light metal matrix composites. *Materials Science and Engineering: A*, *699*, 10–17. https://doi.org/10.1016/j.msea.2017.05.073

Gao, Y., Liu, H., Shi, R., Zhou, N., Xu, Z., Zhu, Y. M., … Wang, Y. (2012). Simulation study of precipitation in an Mg-Y-Nd alloy. *Acta Materialia*, *60*(12), 4819–4832. https://doi.org/10.1016/j.actamat.2012.05.013

Gubicza, J. (2014). *X-Ray Line Profile Analysis in Materials Science*. IGI Global.

University of Malaya

https://doi.org/10.4018/978-1-4666-5852-3

Gubicza, J., Chinh, N. Q., Krállics, G., Schiller, I., & Ungár, T. (2006). Microstructure of ultrafine-grained fcc metals produced by severe plastic deformation. In *Current Applied Physics* (Vol. 6, pp. 194–199). https://doi.org/10.1016/j.cap.2005.07.039

HajyAkbary, F., Sietsma, J., Böttger, A. J., & Santofimia, M. J. (2015). An improved X-ray diffraction analysis method to characterize dislocation density in lath martensitic structures. *Materials Science and Engineering A*, *639*, 208–218. https://doi.org/10.1016/j.msea.2015.05.003

Hempel, N., Nitschke-Pagel, T., & Dilger, K. (2014). Residual stresses in multi-pass butt-welded ferritic-pearlitic steel pipes, 555–563. https://doi.org/10.1007/s40194-015-0230-7

Hempel, N., Nitschke-Pagel, T., & Dilger, K. (2016). Study on the near-surface residual stress state in butt-welded pipes of austenitic steel using X-ray diffraction. *Welding in the World*, *60*(6), 1169–1179. https://doi.org/10.1007/s40194-016-0378-9

Huber, N., & Heerens, J. (2008). On the effect of a general residual stress state on indentation and hardness testing. *Acta Materialia*, *56*(20), 6205–6213. https://doi.org/10.1016/j.actamat.2008.08.029

Jeong, Y., Gnäupel-Herold, T., Barlat, F. G., Iadicola, M., Creuziger, A., & Lee, M. G. (2015). Evaluation of biaxial flow stress based on elasto-viscoplastic self-consistent analysis of X-ray diffraction measurements. *International Journal of Plasticity*, *66*, 103–118. https://doi.org/10.1016/j.ijplas.2014.06.009

Jiang, H. S., Zheng, M. Y., Qiao, X. G., Wu, K., Peng, Q. Y., Yang, S. H., … Luo, J. H.

University of Malaya

(2017). Microstructure and mechanical properties of WE43 magnesium alloy fabricated by direct-chill casting. *Materials Science and Engineering A*, *684*(November 2016), 158–164. https://doi.org/10.1016/j.msea.2016.11.009

Kapoor, K., Lahiri, D., Padmaprabu, C., & Sanyal, T. (2002). X-ray measurement of near surface residual stress in textured cold-worked stress-relieved Zr-2.5%Nb pressure tube material. *Journal of Nuclear Materials*, *303*(2–3), 147–155. https://doi.org/10.1016/S0022-3115(02)00818-8

Kesavan Nair, P., & Vasudevan, R. (1995). Residual stresses of types II and III and their estimation. *Sadhana*, *20*(1), 39–52. https://doi.org/10.1007/BF02747283

Khorsand Zak, A., Abd. Majid, W. H., Abrishami, M. E., & Yousefi, R. (2011). X-ray analysis of ZnO nanoparticles by Williamson-Hall and size-strain plot methods. *Solid State Sciences*, *13*(1), 251–256. https://doi.org/10.1016/j.solidstatesciences.2010.11.024

Kim, W. J., & Jeong, H. T. (2005). Grain-Size Strengthening in Equal-Channel-Angular-Pressing Processed AZ31 Mg Alloys with a Constant Texture. *MATERIALS TRANSACTIONS*, *46*(2), 251–258. https://doi.org/10.2320/matertrans.46.251

Koizumi, T., & Kuroda, M. (2018). Grain size effects in aluminum processed by severe plastic deformation. *Materials Science and Engineering A*, *710*(May 2017), 300–308. https://doi.org/10.1016/j.msea.2017.10.077

Kwak, S. Y., & Hwang, H. Y. (2018). Effect of heat treatment residual stress on stress behavior of constant stress beam. *Journal of Computational Design and Engineering*, *5*(1), 137–143. https://doi.org/10.1016/j.jcde.2017.07.001

University of Malaya

Luo, Q., & Jones, A. H. (2010). High-precision determination of residual stress of polycrystalline coatings using optimised XRD-sin2psi technique. *Surface and Coatings Technology*. https://doi.org/10.1016/j.surfcoat.2010.07.108

Luo, Q., & Yang, S. (2017). Uncertainty of the X-ray Diffraction (XRD) sin2 ψ Technique in Measuring Residual Stresses of Physical Vapor Deposition (PVD) Hard Coatings. *Coatings*, *7*(8), 128. https://doi.org/10.3390/coatings7080128

Maniammal, K., Madhu, G., & Biju, V. (2017). X-ray diffraction line profile analysis of nanostructured nickel oxide: Shape factor and convolution of crystallite size and microstrain contributions. *Physica E: Low-Dimensional Systems and Nanostructures*, *85*, 214–222. https://doi.org/10.1016/j.physe.2016.08.035

Marinkovic, B., Avillez, R. R. De, Saavedra, A., & Assunção, F. C. R. (2001). A comparison between the Warren-Averbach method and alternate methods for X-ray diffraction microstructure analysis of polycrystalline specimens. *Materials Research*, *4*(2), 71–76. https://doi.org/10.1590/S1516-14392001000200005

McKeehan, M., & Warren, B. E. (1953). X-Ray Study of Cold Work in Thoriated Tungsten. *Journal of Applied Physics*. https://doi.org/10.1063/1.1721133

Mesbah, M., Fadaeifard, F., Karimzadeh, A., Nasiri-Tabrizi, B., Rafieerad, A., Faraji, G., & Bushroa, A. R. (2016). Nano-mechanical properties and microstructure of UFG brass tubes processed by parallel tubular channel angular pressing. *Metals and Materials International*, *22*(6), 1098–1107. https://doi.org/10.1007/s12540-016-6152-0

Mesbah, M., Faraji, G., & Bushroa, A. (2014). Characterization of nanostructured pure aluminum tubes produced by tubular channel angular pressing (TCAP). *Materials Science and Engineering A*, *590*, 289–294. https://doi.org/10.1016/j.msea.2013.10.036

University of Malaya

Miller, M. P., & Dawson, P. R. (2014). Understanding local deformation in metallic polycrystals using high energy X-rays and finite elements. *Current Opinion in Solid State and Materials Science*, *18*(5), 286–299. https://doi.org/10.1016/j.cossms.2014.09.001

Mittemeijer, E. J., & Welzel, U. (2008). The "state of the art" of the diffraction analysis of crystallite size and lattice strain. *Zeitschrift Für Kristallographie*, *223*(9), 552–560. https://doi.org/10.1524/zkri.2008.1213

Pamnani, R., Sharma, G. K., Mahadevan, S., Jayakumar, T., Vasudevan, M., & Rao, B. P. C. (2015). Residual stress studies on arc welding joints of naval steel (DMR-249A). *Journal of Manufacturing Processes*, *20*, 104–111. https://doi.org/10.1016/j.jmapro.2015.09.004

Pecharsky, V., & Zavalij, P. (2008). *Fundamentals of Powder Diffraction and Structural Characterization of Materials, Second Edition* (Vol. 26). https://doi.org/10.1007/978-0-387-09579-0

Pourghahramani, P., & Forssberg, E. (2006). Microstructure characterization of mechanically activated hematite using XRD line broadening. *International Journal of Mineral Processing*, *79*(2), 106–119. https://doi.org/10.1016/j.minpro.2006.02.001

Prevéy, P. S. (1986). X-ray diffraction residual stress techniques. *Metals Handbook. 10. Metals Park*, (513), 380–392. https://doi.org/10.1361/asmhba0001761

Reyes-Ruiz, C., Figueroa, I. A., Braham, C., Cabrera, J. M., Zanellato, O., Baiz, S., & Gonzalez, G. (2016). Residual stress distribution of a 6061-T6 aluminum alloy under shear deformation. https://doi.org/10.1016/j.msea.2016.06.016

University of Malaya

Robert W. Cheary, C.C. Tang, P.A. Lynch, M.A. Roberts, S. M. C. (2001). Materials Science Forum Vols . 378-381. *Materials Science Forum*, *378–381*, 254–261. https://doi.org/10.4028/www.scientific.net/MSF.378-381.254

Sanati, H., Reshadi, F., Faraji, G., Soltani, N., & Zalnezhad, E. (2014). Evaluation of residual stress in ultrafine-grained aluminum tubes using shearography. *Proceedings of the Institution of Mechanical Engineers, Part B: Journal of Engineering Manufacture*. https://doi.org/10.1177/0954405414534432

Savaloni, H., Gholipour-Shahraki, M., & Player, M. a. (2006). A comparison of different methods for x-ray diffraction line broadening analysis of Ti and Ag UHV deposited thin films: nanostructural dependence on substrate temperature and film thickness. *Journal of Physics D: Applied Physics*, *39*(10), 2231–2247. https://doi.org/10.1088/0022-3727/39/10/036

Scardi, P., Leoni, M., & Delhez, R. (2004). Line broadening analysis using integral breadth methods: A critical review. *Journal of Applied Crystallography*, *37*(3), 381–390. https://doi.org/10.1107/S0021889804004583

Schajer, G. S. (2013). *Stress Measurement Methods Practical Residual Stress Measurement*.

Scherrer, P. (1918). Estimation of the size and internal structure of colloidal particles by means of röntgen. *Nachr. Ges. Wiss. Göttingen*, *2*, 96–100.

Simm, T. (2013). the Use of Diffraction Peak Profile Analysis in Studying the Plastic Deformation of Metals. *[Thesis]. Manchester, UK: The University of Manchester; 2013.* Retrieved from https://www.escholar.manchester.ac.uk/uk-ac-man-scw:194524

University of Malaya

Simm, T. H., Withers, P. J., & Quinta da Fonseca, J. (2016). An evaluation of diffraction peak profile analysis (DPPA) methods to study plastically deformed metals. *Materials and Design*, *111*, 331–343. https://doi.org/10.1016/j.matdes.2016.08.091

Singh, A., & Agrawal, A. (2015). Investigation of surface residual stress distribution in deformation machining process for aluminum alloy. *Journal of Materials Processing Technology*, *225*, 195–202. https://doi.org/10.1016/j.jmatprotec.2015.05.025

Sivakami, R., Dhanuskodi, S., & Karvembu, R. (2016). Estimation of lattice strain in nanocrystalline RuO<inf>2</inf> by Williamson-Hall and size-strain plot methods. *Spectrochimica Acta - Part A: Molecular and Biomolecular Spectroscopy*, *152*, 43–50. https://doi.org/10.1016/j.saa.2015.07.008

Toth, L. S., & Gu, C. (2014). Ultrafine-grain metals by severe plastic deformation. *Materials Characterization*, *92*, 1–14. https://doi.org/10.1016/j.matchar.2014.02.003

Tromans, D. (2011). Elastic Anisotropy of HCP Metal Crystals and Polycrystals. *Ijrras*, *6*(March), 462–483.

Umansky, Y. S., Skakov, U. A., Ivanov, A. N., & Rastorguev, L. N. (1982). Crystallography, X-ray and electron microscopy. *Metallurgy, Moscow*, *632*.

Ungár, T., Balogh, L., & Ribárik, G. (2010). Defect-related physical-profile-based X-ray and neutron line profile analysis. *Metallurgical and Materials Transactions A: Physical Metallurgy and Materials Science*, *41*(5), 1202–1209. https://doi.org/10.1007/s11661-009-9961-7

Ungár, T., Castelnau, O., Ribárik, G., Drakopoulos, M., Béchade, J. L., Chauveau, T., … Bacroix, B. (2007). Grain to grain slip activity in plastically deformed Zr determined

University of Malaya

by X-ray micro-diffraction line profile analysis. *Acta Materialia*, *55*(3), 1117–1127. https://doi.org/10.1016/j.actamat.2006.09.031

Ungár, T., Dragomir, I., Révész, Á., & Borbély, A. (1999). The contrast factors of dislocations in cubic crystals: The dislocation model of strain anisotropy in practice. *Journal of Applied Crystallography*, *32*(5), 992–1002. https://doi.org/10.1107/S0021889899009334

Ungár, T., Gubicza, J., Hanák, P., & Alexandrov, I. (2001). Densities and character of dislocations and size-distribution of subgrains in deformed metals by X-ray diffraction profile analysis. *Materials Science and Engineering A*, *319–321*, 274–278. https://doi.org/10.1016/S0921-5093(01)01025-5

Ungár, T., & Tichy, G. (1999). The effect of dislocation contrast on X-ray line profiles in untextured polycrystals. *Physica Status Solidi (A) Applied Research*, *171*(2), 425–434. https://doi.org/10.1002/(SICI)1521-396X(199902)171:2<425::AID-PSSA425>3.0.CO;2-W

Venkateswarlu, K., Chandra Bose, A., & Rameshbabu, N. (2010). X-ray peak broadening studies of nanocrystalline hydroxyapatite by WilliamsonHall analysis. *Physica B: Condensed Matter*, *405*(20), 4256–4261. https://doi.org/10.1016/j.physb.2010.07.020

Vermeulen, A. C. (2006). Considerations for Collecting Reliable Xrd Residual Stress Data Across the Full 2Theta Range. *JCPDS -International Centre for Diffraction Data*, 133–142.

Warren, B. E. (1969). X-ray Diffraction.,(1969). *Reading, MA: Addison-Wesley Pub. Co*, *7*, 381.

University of Malaya

Waseda, Y., Matsubara, E., & Shinoda, K. (2011). *X-Ray Diffraction Crystallography*. https://doi.org/10.1007/978-3-642-16635-8

Wilson, A. J. C. (1963). *Mathematical theory of X-ray powder diffractometry*. Philips technical library Eindhoven.

Withers, P. J., & Bhadeshia, H. K. D. H. (2001). Residual stress. Part 1 – Measurement techniques. *Materials Science and Technology*, *17*(4), 366–375. https://doi.org/10.1179/026708301101510087

Withers, P. J., Preuss, M., Steuwer, A., & Pang, J. W. L. (2007). Methods for obtaining the strain-free lattice parameter when using diffraction to determine residual stress. *Journal of Applied Crystallography*, *40*(5), 891–904. https://doi.org/10.1107/S0021889807030269

Zhang, Z., Zhou, F., & Lavernia, E. J. (2003). On the analysis of grain size in bulk nanocrystalline materials via X-ray diffraction. *Metallurgical and Materials Transactions A-Physical Metallurgy and Materials Science*, *34A*(6), 1349–1355. https://doi.org/10.1007/s11661-003-0246-2

Zhu, Y. T. (2006). Deformation twinning in nanocrystalline fcc copper and aluminum. In *Nanostructured Materials by High-Pressure Severe Plastic Deformation* (pp. 3–11). Springer.

University of Malaya